1-1-2002

Evaluation of a moving bed granular filter in conjunction with a biomass gasifier

Joshua Stevan Nunez
Iowa State University

Evaluation of a moving bed granular filter in conjunction with a biomass gasifier.

by

Joshua Stevan Nunez

A thesis submitted to the graduate faculty

in partial fulfillment of the requirements for the degree of

MASTERS OF SCIENCE

Major: Mechanical Engineering

Program of Study Committee:
Robert C. Brown (Major Professor)
Ron M. Nelson
Steven J. Hoff

Iowa State University

Ames, Iowa State University

2002

Graduate College
Iowa State University

This is to certify that the master's thesis of

Joshua Stevan Nunez

has met the thesis requirements of Iowa State University

Signatures have been redacted for privacy

TABLE OF CONTENTS

LIST OF FIGURES

LIST OF TABLES

ACKNOWLEDGEMENTS

This thesis was prepared with the support of the U. S. Department of Energy (DOE) under Award No. DE-FG26-99FT40588. However, any opinions, findings, conclusions, or recommendations expressed herein are those of the author(s) and do not necessarily reflect the views of the DOE.

I would like to give special thanks to my major professor, Dr. Robert C. Brown. His guidance, kind words, and encouragement during frustrating times made it possible for me finish this project. It is a great feeling to finally be done!

I would also like to thank all of the people who helped in the set-up, collection, and analysis of the MBGF data. Thanks Keith Cummer, Daren Daugard, Brad Dvorak, Jim Pollard, Huawei Shi, Jerod Smeenk, Dave Starks, and Andy Suby.

I would like to express my love and gratitude to my wonderful girlfriend, Jennifer Gray, who has been more than understanding during this entire process. Thanks! I would also like to thank my family, Steve, Roberta, and Ross Nunez. Thanks for your words of encouragement and advise.

ABSTRACT

A moving bed granular filter (MBGF) was tested for the removal of particulates from a high temperature producer gas of a biomass gasifier. As a result of problems in high temperature isokinetic sampling, the efficiency of the MBGF was not accurately determined. However, it appears that the inlet concentration to the MBGF was in the range of 2 to 30 g/m^3, with the most likely level being around 5 g/m^3. There are several indications clues that indicate that the MBGF was working at relatively high efficiency, although this could not be quantified. Particulate analysis under the scanning electron microscope (SEM) showed no traces of silicon, a major component of the filter media, which disproved a concern that the MBGF was adding dust from the granular media to the producer gas stream. The SEM results also showed that the MBGF effectively removed most of the largest particulate from the entering gas stream, which suggests filtration to some degree. Additionally, an analysis of the waste MBGF filter media showed that up to 5 g/m^3 of dust was being removed from the entering stream. All of these results point toward a reasonable level of filtration.

CHAPTER 1: INTRODUCTION

Biomass gasification has been used primarily for heat generation, but has the potential to be used for electrical generation. One obstacle limiting this technology from becoming a feasible method of power generation is the lack of an effective particulate removal system. The challenges require the particulate removal method be continuously operating at a high temperature. In addition, pressure drop must be low to minimize impact on overall system performance. High temperature particulate removal is desired for power generation, because cold gas cleaning wastes thermal energy.

Granular filters are well known for their high collection efficiencies at high temperatures [1]. These filters have typically operated in the following modes: fixed bed and continuously moving bed [2]. Continuously moving bed filters or moving bed granular filters (MBGF) are becoming more appealing as a means of particulate removal in biomass gasification. This is especially true for high temperature applications where other particulate removing technologies (i.e. bag house filters, ceramic filters, electrostatic precipitators, and cyclones) fall short.

A MBGF suitable for dry scrubbing a high temperature product gas from biomass gasification has been developed. This innovation will be tested with producer gas from a 4,500 kg-per-day (4.5 tonne-per-day) fluidized bed gasifier. The filter is intended to remove particulate from producer gas with high efficiency and low-pressure drop. Additionally, tar and other contaminants including alkali may be reduced depending on filter media and operating temperature.

CHAPTER 2: BACKGROUND

Many types of filters have been utilized in reducing particulate loading in gaseous streams. Some of the most common filters used in high temperature and/or combustion applications include barrier filters, electrostatic precipitators, cyclone dust collectors, and granular filters. All of these filters incorporate one or more of the following collection mechanisms: interception, inertial impaction, diffusion, gravity, and electrostatic deposition. Assuming that a single particle is used to collect particles entrained in a streamline, brief explanations for the five collection mechanisms are found below. Further details can be found in [3], [4], and [5].

Single-particle collection mechanisms

Interception is more prevalent with smaller particles that do not have significant inertia. As a result, these small particles follow the streamlines of the gas stream. Likewise, as these particles flow past a single particle they sometime touch the filter particle and become attached. This mechanism removes the particles from their respective streamline. Interception does not depend on the streamline velocity.

As its name implies, *inertial impaction* is a result of a particle's inertia. Namely, this collection mechanism is most common for large particles with high inertia. As streamlines flow around a granule or fiber in a filter, large, heavy dust particles are not able to follow the streamline. Thus, they impact the filter granule or fiber and are removed from their original streamline. The governing equation for this collection mechanism is the Stokes number. This dimensionless number is defined as:

$$Stokes\ Number = \frac{\rho_p D_p^2 VCu}{9\mu D_m} \qquad (1)$$

where ρ_p is the particulate density, D_p is the particulate diameter, velocity, V, Cunningham correction factor, Cu, fluid viscosity, μ, and filter media diameter, D_m are used to determine the Stokes Number. With increasing Stokes number one can expect greater collection.

Diffusion is most common for very small particles, which do not follow streamlines very well and, as a result, move in various directions. This random movement of a particle is often referred to as Brownian motion. This motion can increase the probability of dust collection on a single particle. Diffusion is a function of the Peclet number, which is defined as:

$$Pe = \frac{d_f V_o}{D} \qquad (2)$$

where d_f is the particle fiber diameter, V_0 is the superficial velocity, and D is the particle diffusion coefficient.

Gravitational collection occurs when heavy particles settle out of a streamline as result of gravity. This collection is seen more in low flow situations.

Electrostatic deposition occurs when strong electrostatic fields are applied to a dust-laden stream. In order for this collection mechanism to work the dust particles must carry a charge.

Most of these mechanisms for particulate collection are present to some degree in moving bed granular filters (MBGF). However, it should be noted that inertial impaction is

the most dominant mechanism for removing particulate for most situations typical of combustion and gasification systems.

Barrier filters

There are various types of barrier filters, which include baghouse collectors and ceramic filters. Ceramic filters are most commonly used for high temperature applications whereas baghouse filters are typically used in lower temperature applications. These filters are considered barrier filters because a gas stream is passed through the filter and it retains most of the dust from passing through the tightly woven filter fabric. Figure 1 demonstrates the collection mechanism for barrier filters [6].

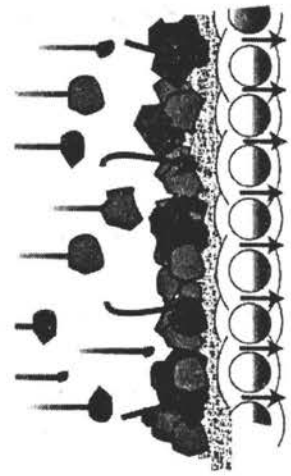

Figure 1: Barrier filter collection mechanism

As one can see from the figure above, the barrier filter does not allow particulate to pass through the filter. However, this filter does not remove all of the particulate initially. Initially the filter only collects the larger particulates while allowing the smaller particulate (i.e. smaller than the interstitial voids of the media) to pass through the filter. Prolonged operation of the filter leads to the formation of a dust cake or a thin layer of particulate

matter, which in increases the filter's particulate collection efficiency greatly. However, this accumulation increases the pressure drop over time. Therefore, a back pulse of air or other means is necessary to remove the dust cake in order to maintain the filter for prolonged operation.

Baghouse filters

Baghouse filters are commercially available. Standard baghouse filters can accommodate flow rates from 0.10 to 50 standard cubic meters per second (200 to 100,000 SCFM). Custom baghouse filters can handle up to 500 standard cubic meters per second (1,000,000 SCFM). Depending on the temperature of the application, filters can be made from nylons, polyesters, fiberglass, and Teflon. They have been used in utility boilers and can operate in temperatures up to 290 °C (550 °F).

Drawbacks to barrier filters include a requirement for low face velocities, inadequate mechanical strength and chemical inertness, complexity of cleaning the filter, low operating temperatures, and inability to operate in moist environments [7]. Although these types of filters are very effective in certain applications, they are less desirable for high temperature gas cleaning and high flow conditions.

Ceramic filters

Many different types of ceramic filters exist, which include woven bags, felt bags, candles and membrane cross-flow filters. Favorable characteristics include suitability for high temperature applications 1093 °C (2000 °F), high resistance to thermal shock, chemically resistant to corrosive gases, and their high collection efficiencies. Woven

ceramic bags are recommended to operate between 0.015 to 0.025 m/s (3 to 5 ft/min) [8]. Other ceramic filters can also be expected to operate within the same velocities.

Their collection mechanisms follow the same collection mechanisms as baghouse filters. Additionally, they follow the same principles of operation, which require intermittent back pulses of air to remove the dust cake formed on the media surface. Ceramic candles and cross-flow filters have difficulties removing particulate during operation while woven and felt bags often encounter problems associated with mechanical strength.

Electrostatic precipitators

An electrostatic precipitator (ESP) is an effective way to remove particulate matter over a particle range from about 10 μm down to 0.01 μm, or even 0.001 μm from an air or gas stream [9]. ESPs were first deigned in 1907 by Dr. Frederick Cottrell. Since then ESPs have been utilized in industry, coal-fired electric power plants, and residential applications to remove particulate matter.

Electrostatic precipitators remove particulate matter through the use of electrostatic forces. An ESP consists of a discharge electrode (negative charge) and a collection plate (positive charge) [10]. Figure 2 demonstrates the particle collection process. High voltage on the order of 30 kV is passed through the discharge electrode where a corona discharge is generated. The corona discharge creates a strong negative electric field where passing gas molecules are ionized. These ions drift through the gas and attach themselves to any particulate matter that they encounter. As a result the particulate becomes negatively charged by the ion, repelled by the strong negative electric field, and attracted to the positive collector plates. On the collector plate surface the particulates accumulate until they are mechanically

removed through vibration or fall via gravity into a collection hopper. This process results in a dry dust, which is makes disposal of the particulate matter easy. However, during the process of vibration there exists the potential for some of the particulate matter to be reintroduced in the gas stream, which can decrease collection efficiencies. Use of a wet ESP can eliminate the problem of reintroducing particulate, but introduces a new problem of disposing of waste slurry. Figure 2, courtesy of PowerSpan Corporation [11], shows the separation theory of an ESP.

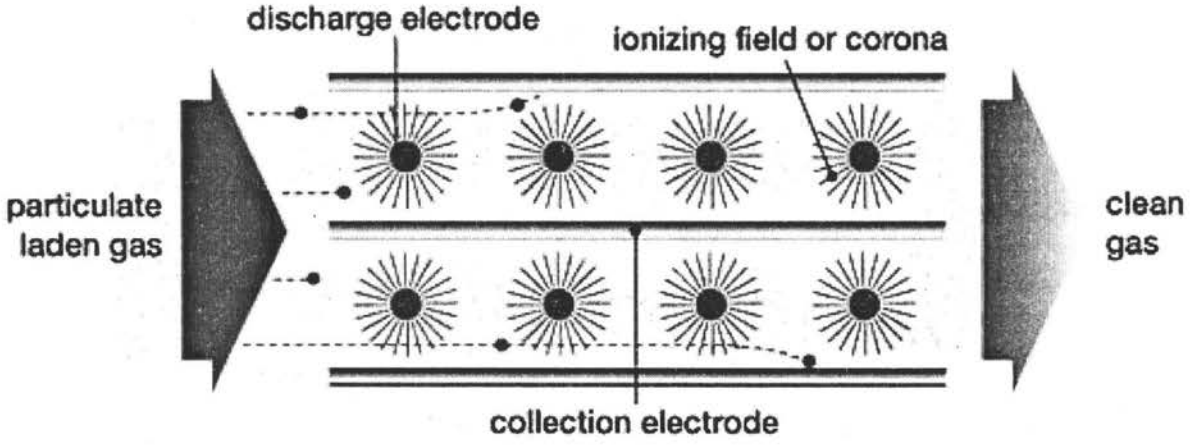

Figure 2: Electrostatic precipitator particulate separation theory

Reported collection efficiencies for ESPs have ranged from 90-99.9%. Low pressure drops, which are typically less than 13 mm H_2O (0.5 in H_2O), and ability to collect dry particulate are appealing attributes to ESPs [12]. However, their high capitol costs, sensitivity small changes in operating conditions (i.e. temperature, gas flow rate, gas composition, and particulate loading) makes them less desirable. Additionally, dust particles with high resistivities are not easily charged and do not separate well in ESPs. Although

there exists some ESPs that are able to operate under 450 °C, no commercial ESPs exist for applications above this range [13].

Cyclone dust collectors

Cyclones are a simple way to separate particulate matter from a gaseous stream. There are various types of cyclones that are available, but axial flow cyclones and tangential inlet cyclones are most popular. This section will only review the tangential inlet cyclone, which is shown below in figure 3.

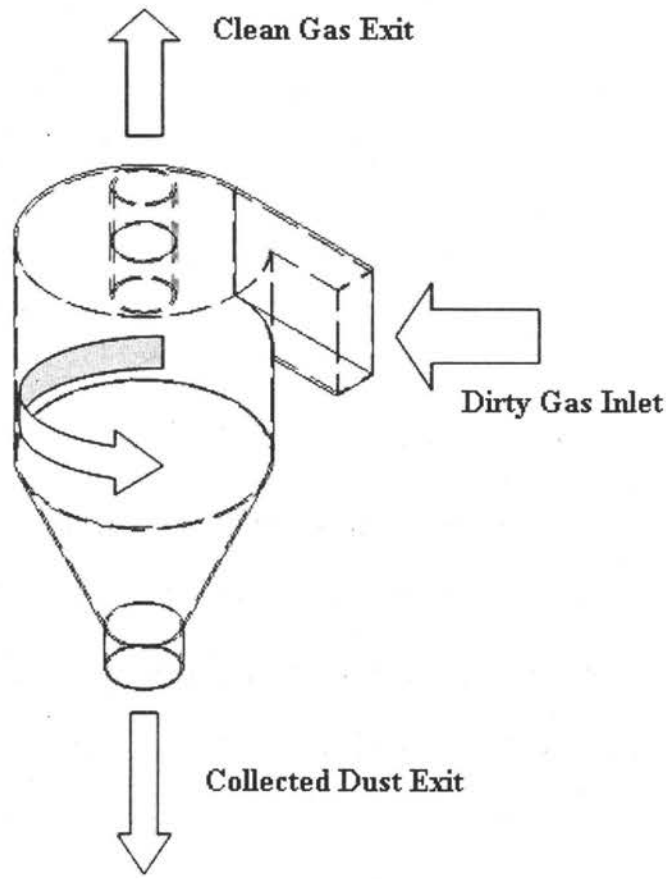

Figure 3: Tangential inlet cyclone schematic

Cyclones remove particulate matter through centrifugal forces. Particulate laden gas enters the cyclone tangentially, which results in a centrifugal force that pushes the large particles (greater than 10 μm) towards the cyclone wall. Figure 4 demonstrates the separation of gas and particulate matter within the gas stream.

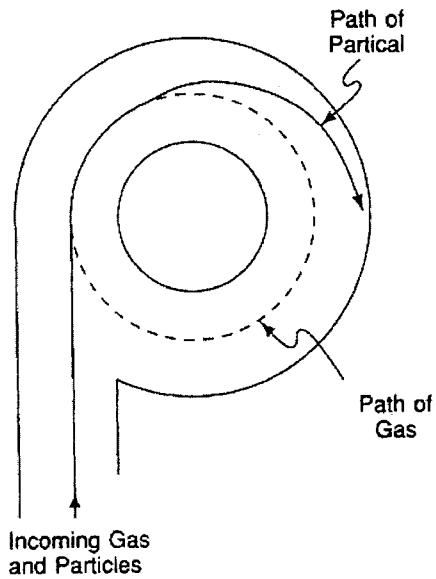

Figure 4: Gas and particle movement in a cyclone

After separation, the relatively clean gas continues to flow radially downward until it reaches the bottom of the cone and then proceeds to travel upward and exits the cyclone. Most of the particulate matter is separated shortly after the gas enters the cyclone. This particulate matter is collected on the walls of the cyclone and travels to the bottom of the cyclone where it is stored and disposed of properly.

Cyclones are very appealing for particulate removal for their simplistic design, which lack moving parts. Some additional advantages of a cyclone include low capitol costs, small space requirements, dry particulate collection and disposal, relatively high temperature

operation, and low pressure drop. Disadvantages include their inability to removal small particulates with high efficiencies. Higher collection efficiencies often require use of multiple cyclones, which results in increased pressure drop. As a result of this restriction, increased power requirements of the system are required.

Since cyclones are not able to effectively remove all particulate less than 10 μm from a gas stream, they should not be used as the only particulate removal device. Instead they may serve as a preconditioning device for another filter that can effectively remove a wide range of size distributions.

Moving bed granular filter (MBGF)

The principle of using a volume of granules to filter a dirty gas is at least 80 years old [14]. Typically granular-beds have been utilized under two different operating conditions: fixed-bed and continuously moving bed filters. Fixed bed filters require periodic cleaning or back pulses as the filter media becomes saturated with particulate and the pressure drop across the filter increases. Moving bed granular filters do not require periodic cleaning or maintenance. Given their operation of continuously replacing dirty filter media they are able to run without increased pressure drops and cleaning for extended periods of time.

Squires and Pfeffer [15] were among the first to consider the use of granular beds for control of fly ash emissions. Reported collection efficiencies were as high as 99.8%. Lippert and coworkers [16] reported collection efficiencies of essentially 100% for fixed beds operated at superficial velocities less than 0.4 m s^{-1} (1.31 ft s^{-1}). Significantly, they attributed these outstanding results to the formation of a dust cake at the surface of the beds, a result confirmed by tests with Plexiglas models operated at ambient conditions. It was

hypothesized that dust bridges the gaps between individual media granules and the collection mechanism shifts from interception deep within the bed to impaction at the freeboard-bed interface.

Moving bed filters date back to the 1940's [17]. Some of the earliest designs employed cross-flow configurations. The Dorfan Impingo filter [18], offered commercially in the 1950's, used 1.3 cm (0.51 in.) to 3.8 cm (1.5 in.) pebbles enclosed in 30 cm (11.8 in.) thick panels. Several decades later, the Combustion Power Company developed a cross-flow filter in which the gas flowed radially outward through an annular moving bed of 3 mm (0.12 in.) to 6 mm (0.24 in.) pea gravel [19]. Plugging of the screens that enclosed the granular media was often a problem in this design. Combustion Power Company went on to develop a screenless MBGF to avoid plugging problems [20]. The resulting design appears to be the first parallel flow MBGF. Granular material was fed to the surface of the bed through a complex of eight, gravity-fed pipes. Collection efficiency was 99% for particulate greater than 4 μm diameter and exceeded 93% for smaller particulate. Some of the literature published on this filter suggests that most of the particulate capture occurred in a zone very close to the injection point of gas into the bed.

Based on observations by other researchers that formation of a dust cake is important to efficient particulate collection for fixed bed granular filters, Brown et al. have developed a new concept for a MBGF that makes use of this phenomenon [21]. The goal is to establish a quasi-steady dust cake that is continuously or periodically renewed on the upstream side of the dust cake and swept away on the downstream side.

In the new filter design, granular material moving downward by gravity spills from a centrally located dipleg to form an interfacial region where dust cake forms and most

particulate removal occurs. The lower edge of the filter cake is dispersed by the downward flow of granular material while the upper interface is continuously covered by a fresh layer of granular material cascading from the dipleg above the interface. In this fashion, the interface establishes a dust cake of quasi-steady thickness, which is controlled to give high collection efficiency and acceptable pressure drop.

The filter includes three innovations in the development of a new MBGF [19]: a *tangential gas inlet*, a *flow straightening section*, and a *screened gas disengagement section*. These sections can be seen in figure 5.

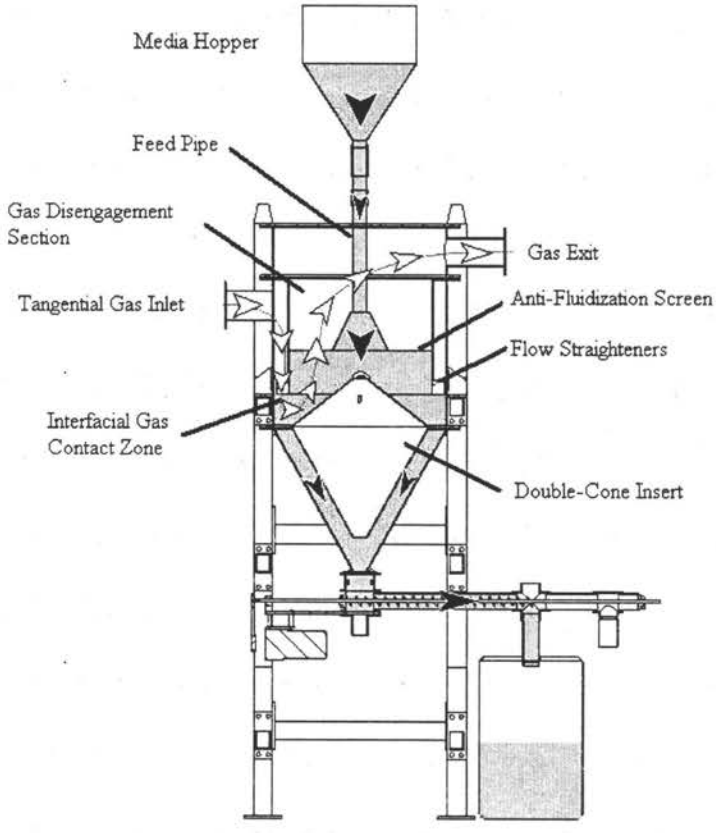

Figure 5: Schematic of MBGF

As illustrated in figure 5, the gas enters the filter through a *tangential gas inlet*, which imparts a cyclonic motion to the gas flow. Inside the filter, the gas swirls downward towards

the interface between the gas and granular bed. By imparting cyclonic flow, the momentum of the gas is preserved, reducing pressure drop normally associated with sudden expansion into a filter. However, granules and dust cake on the surface of the filter bed would be disturbed unless the radial component of the gas flow is redirected in the axial direction before the gas reaches the bed surface.

A *flow straightening section*, consisting of evenly spaced fins distributed radially about the circumference of the annular space above the surface of the bed, redirects the flow downward. The flow-straightening section also evenly distributes the gas flow over the surface of the bed, which is important to the efficient utilization of the filter media. Gas cleaning is hypothesized to occur primarily at this interface. The accumulation of dust particles on the granules and in the voids between granules forms a thin dust cake, which aids in the capture of particulate in the gas flow.

The *gas disengagement section* requires a special configuration to allow high gas flows through the filter. The upward flowing gas induces a drag on the granules that causes the bed to expand and eventually fluidize, an undesirable behavior that limits gas throughput for the filter. The gas disengagement section consists of a small diameter feeder tube conveying granular material to a larger diameter down-comer. At low gas velocities, the granules from the feeder tube spread out into a conical pile much like the one in the engagement section. However, at high gas velocities, these particles expand upward against an annular porous plate or screen that prevents their continued expansion. The screen allows gas to exit the filter while retaining granular material.

These innovations were incorporated into a pilot-scale filter that is being tested with producer gas from a 4,500 kg-per-day (4.5 tonne-per-day) fluidized bed gasifier.

CHAPTER 3: EXPERIMENTAL SET-UP

Gasifier size and description

A pilot-scale fluidized bed reactor, illustrated schematically in figure 6, was used to generate the particulate-laden producer gas used in these experiments. The gasifier is rated at 800 kW (2.8 MMBtu hr^{-1}) thermal input, which corresponds to an average throughput of 180 kg hr^{-1} (400 lb hr^{-1}) of biomass fuel at a heating value of 16,300 kJ kg^{-1} (7000 Btu lb^{-1}). The nominal gas generation rate is 340 nm^3 h^{-1} (200 sft^3 min^{-1}).

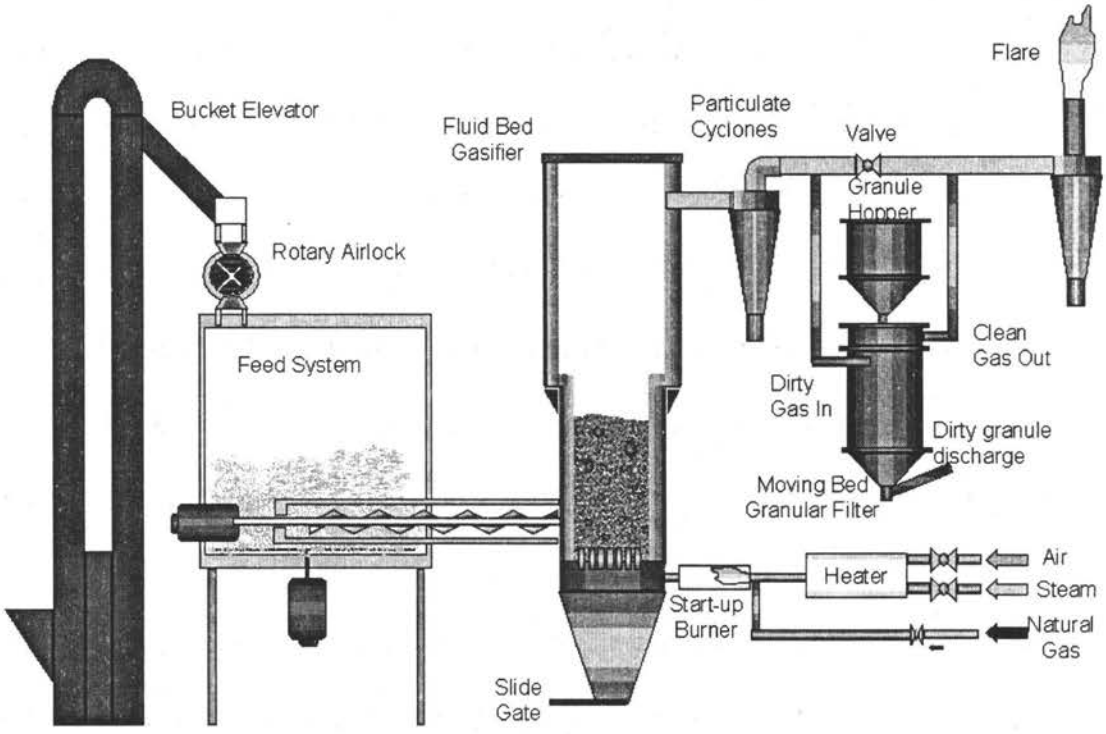

Figure 6: Gasifier Schematic

The experiments employed a mixture of waste seed corn and waste soybean seed as fuel, which are waste streams of interest to one segment of the agricultural processing industry. Other biomass feed stocks such as switch grass, corn stover, and wood chips could

also be utilized as a fuel, but were not incorporated into these experiments. A variable speed auger metered fuel from a hopper into a constant-speed injection auger. The constant-speed auger injected the fuel into the bottom of the fluidized bed. To prevent the backflow of hot gases into the fuel injection auger, pressurized air is inserted to help reduce the amount of hot gas that comes into the into the injection auger. If hot gases were allowed to come into contact with the fuel this would cause the fuel to gum up in the auger, which would eventually clog the injection auger.

The fluidized reactor measures 46 cm (18 in) in diameter and stands 3.7 m (12 ft) tall. The reactor wall is lined with castable ceramic to insulate the vessel for increased thermal efficiency. Fluidization air enters the reactor through an array of nozzles that evenly distribute air to the bottom of the bed. The bed media consisted of sand mixed with a small quantity of limestone to minimize agglomeration of bed material arising from alkali in the biomass feed. Particulate-laden producer gas exited the reactor through the freeboard and passes through a cyclone that removes much of the particulate matter larger than 10 μm in size. Details on the operation of the biomass gasifier can be found in Smeenk and Brown [22].

The bed of sand and limestone was fluidized with air at an equivalence ratio between 0.25 and 0.30, which maintained the bed in the temperature range of 700 to 760 °C (1,290 to 1,400 °F). An equivalence ratio is defined as the ratio of the mass flow rate of air to the mass flow rate of fuel. The feed rate of biomass during these trials was in the range of 150 to 180 kg/h (325-400 lb/h).

MBGF description

Upon leaving the cyclone, the hot producer gas entered the MBGF. The filter, as illustrated previously in Fig. 5, consisted of five major sections: a cyclonic inlet, a flow straightening section, an interfacial gas contacting region, a granule down-comer, and a gas disengagement section. The cyclonic gas inlet imparts a radial component to the gas flow for the purpose of reducing entrance pressure losses. This inlet consists of a 0.914 m (36 in) diameter cylinder of 0.762 m (30 in) length constructed of mild steel. Once inside the MBGF, the hot gas swirls radially downward until it reaches a flow straightening section. This section serves to redirect the gas uniformly and perpendicularly into the gas-contacting region while preventing the reintroduction of deposited particulate. Each of the 80 flow straighteners measure 0.076 m (3 in) long and 0.07 m (2.6 in) wide. Particulate is filtered from the gas flow in the interfacial region immediately below the fins. After passing through the interfacial region, the clean gas flows upward through the granule down-comer until it reaches the disengagement section. The disengagement section consists of a 0.76 m (30 in) diameter cylinder of 0.61 m (24 in) length constructed of mild steel. A stainless steel mesh screen retains granular material and prevents the moving bed from fluidizing. Without this screen, the bed would continue to expand increasing the void space and allowing some of the particulate that was not caught at the cake to short circuit through the bed.

Granular material is gravity fed to the filter from a feed hopper above the filter by means of a 0.07 m (3 in) diameter delivery pipe that passes through the center of the stainless steel mesh screen. Gas does not flow into the delivery pipe because feed hopper is sealed. The capacity of the filter is 0.45 m^3 (15.9 ft^3) while that of the hopper is 0.15 m^3 (5.35 ft^3). Dust-laden granular material exiting the bottom of the filter is augured into a barrel for

subsequent disposal. Waste granular media is augured horizontally into a 0.20 m^3 (7.35 ft^3) barrel. The 5.08 cm. (2 in.) auger is belt-driven by a high torque gear motor. The belt-driven pulley system helps to insure that high loads will not damage the gear motor.

Isokinetic sampling system

To accurately determine the particulate loading of the producer gas stream, it was necessary to isokinetically sample gas. Isokinetic sampling is a procedure that ensures a representative sample of particulate enters a sample probe when sampling from a moving gas stream [23]. However, the method is prone to gross sampling errors if not properly performed. Figure 7, shows the streamline of the gas and the respective sampling conditions.

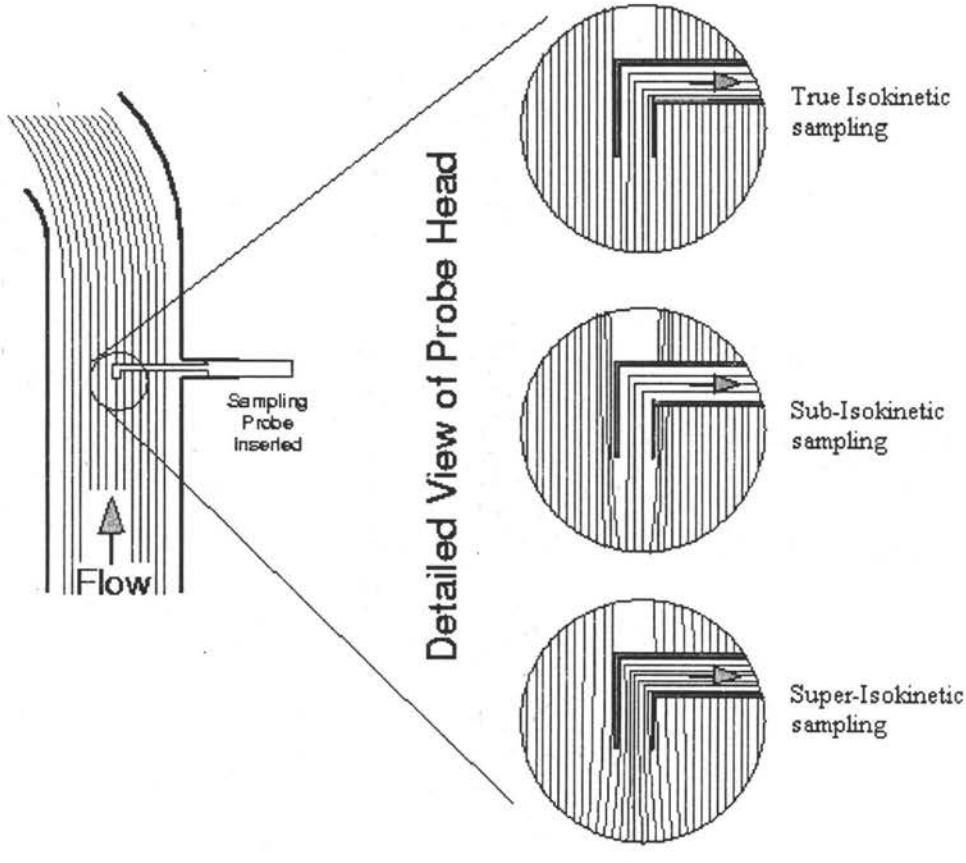

Figure 7: Isokinetic Sampling conditions
(Figure courtesy of Air Flow Sciences [24])

True isokinetic sampling occurs when the sampling velocity equals the gas stream velocity. A true isokinetic sampling condition removes a representative volume of gas along with the particulate. All particles follow their respective streamlines into the sample probe without disturbances.

Sub-isokinetic sampling occurs when the sampling velocity is less than the streamline velocity. This forces the streamlines to bend around the sample probe, which can effect the collection of particulate and dust concentrations. This can be seen in figure 7. Larger particles tend not to follow their respective streamlines as a result of their high inertia. Therefore they are not able to bend around the sample probe as the streamlines and are collected. The collection of these high mass particles and the less-than-isokinetic volume of gas sampled results in measured concentrations that are higher than actual dust concentrations.

Super-isokinetic sampling results when the sampling velocity is greater than the streamline velocity. This condition forces the streamlines to bend towards the sample probe, which can also effect the collection of particulate and dust concentrations. Figure 7 illustrates this condition well. As seen in sub-isokinetic sampling, the large particles behave in the same manner. The only difference being the volume of gas sampled. An increased volume of gas tends to result in measured concentrations that are lower than actual dust concentrations and potentially a higher collection of smaller particles. Sub-isokinetic and super-isokinetic sampling conditions should be avoided.

The sampling systems upstream and downstream of the MBGF (designated as the inlet and exit sampling systems, respectively) are designed to separately capture particulate and tar as well as measure gas composition. As illustrated in figure 8, each sampling system

consists of a sample probe, a heated sintered-metal particulate filter, an impinger train to collect tar, a vacuum pump, a rotameter, and a volumetric gas meter. Additionally, gas exiting the vacuum pumps can be directed to a Varian Model CP2003 Micro-Gas Chromatograph for determination of gas composition. Although gas compositions were not needed for determining the efficiency of the MBGF, the results added confidence in sampling procedures through the detection of oxygen. The presence of oxygen in the sample lines is indicative of a leak since producer gas is typically free of oxygen.

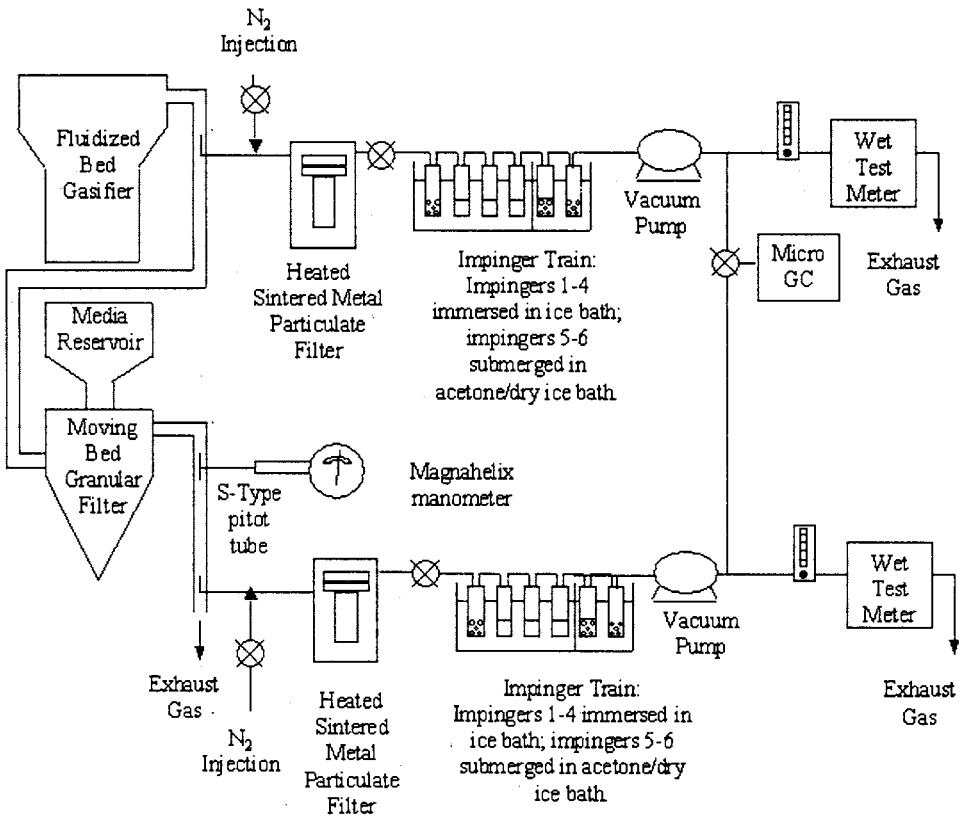

Figure 8: Isokinetic Sampling Schematic.

Accurate quantification of particulate loading in the producer gas entering and exiting the MBGF mandates the use of isokinetic sampling. The velocity in the producer gas duct downstream of the MBGF was measured with an S-type pitot [25] tube suitable for high

particulate applications from United Sensor Corporation. The pitot tube was located downstream of the MBGF to help minimize the amount of particulate it experienced, which helped prevent plugging. The velocity from the pitot tube was temperature corrected for the of inlet and exit particulate sampling probes. Isokinetic sampling was obtained by matching the velocity at the tip of the sampling probe with the velocity in the producer gas duct. Both isokinetic sample probes and the pitot tubes were held at a constant location. A uniform particulate distribution and velocity profile were assumed to be constant across the exhaust duct. The average gas velocity in the probe was calculated by dividing the volumetric flow rate in the sampling line, as measured with a Cole Parmer Flowmeter, by the cross-sectional area of the sampling probe.

The isokinetic flow rates were determined through a MathCad program that used the operating conditions of the MBGF. These included the pitot tube pressure differential, pitot tube temperature, and the temperature of the sample location. A copy of the MathCad program used to determine the isokinetic flow rates can be found in Appendix A. The isokinetic flow rate was monitored throughout the test and corrected as the operating conditions changed with time.

Gravimetric analysis was used to determine particulate loading of the gas stream. This method assumed that the filter holder and filter element did not change weight during a test as the result of temperature, chemical exposure, or handling. Sampling filters of low pressure drop were preferred as this allowed for longer sampling periods without concern for filter plugging and increased pressure drops associated with plugging. Therefore, appropriately sized sintered metal filters were chosen to determine the dust loading of the MBGF. Initial testing employed a Mott 6300 Series sintered metal filter downstream of the

MBGF, which consisted of 7 individual porous cups filter utilized a carbon fiber gasket. This filter was chosen for its reduced weight, which was thought to help reduce the errors in mass measurements. Also employed was a Mott Hyline Series cylindrical, stainless steel 316, sintered metal filter of 0.06 m (2.5 in) diameter and 0.23 m (9 in) length, designed with 0.5 μm cut-size. As testing progressed, it became obvious that the set-up and teardown procedure for the Mott 6300 filter was very complex, which allowed for additional user error. The filter also experienced plugging, which led to replacement of the Mott 6300 filter with a Mott Hyline Series cylindrical filter in both sample lines.

The filters were operated in ovens maintained at 450 °C (842 °F) to prevent condensation of tars, which are high molecular weight organic compounds. These viscous compounds would have plugged filter pores as well as made it difficult to distinguish between tar and particles. In addition, sample lines upstream of the impinger trains were heated to 450 °C (842 °F) with Cole Palmer ½ inch Dual-Element heating tapes.

Both sample lines provided quantitative measurement of various tar fractions by means of six glass impinger bottles [26]. The first four bottles were immersed in an ice bath while the last two bottles were immersed in an acetone/dry ice bath. The first and sixth bottles were filled with glass beads, while the second, third and fourth bottles were filled with dichloromethane. The fifth bottle was filled with both glass beads and dichloromethane. The gas leaving the impinger trains passed through diaphragm vacuum pumps before exiting through volumetric gas meters to accurately determine the total gas volume sampled.

Sample location

In order to accurately measure the velocity in a duct one must perform a traverse at the desired sample location. Traversing is a technique used to find the average velocity in the duct. Taking velocity measurements at specified locations throughout the cross-sectional area of the duct gives an average velocity. The shape and size of the duct determines the method of traversing, which may include the log-Tchebycheff rule or the equal area method where the former has more accuracy [27]. In addition to determining the average velocity, traversing is a good indicator of whether or not the velocity profile is flat. In performing a traverse, one must locate the sample location 7.5 duct diameters downstream of any disturbance and 3 duct diameters upstream of any disturbance [37]. This helps to insure that the flow profile is fully developed, which acts to increase accuracy in the measurement.

Before sampling commenced, the 15.24 cm (6 in) exhaust ducts leading to and from the MBGF were traversed, eight measuring points were made on 2 perpendicular axes. Both upstream and downstream duct diameter constraints were met and the results were indicative of a flat profile. Therefore, the sample probes were set in the middle of the duct.

Additionally, since the effect of buoyancy driven flows was not known, calculations were performed to determine the buoyancy effects in the vertical exhaust pipes. The following calculation was performed to see if buoyancy effects could be neglected. The Grashoff number, or the ratio of the buoyancy force to the viscous force acting on the fluid can be found in equation (3) while the Reynolds number found in equation 4. The ratio of the Grashoff to Reynolds squared is found in equation 5 and can serves as a good indicator of whether or not buoyancy effects can be neglected [28].

$$Gr = \frac{gB(T_s - T_\infty)L^3}{\upsilon^2} \quad (3)$$

$$\mathrm{Re} = \frac{U_o L}{\upsilon} \quad (4)$$

$$\frac{Gr}{\mathrm{Re}^2} << 1 \quad (5)$$

Where g is the gravitational constant, β is the expansion coefficient, T_S is the duct temperature, T_∞ is the surrounding temperature, L is the duct diameter, U_o is the velocity, and υ is the viscosity. Equation (5) was found to be much less than 1, which indicates that the effects of buoyancy could be neglected.

Filter media disposal

The dirty filtering media was disposed of at the local landfill. However, the filtering media, in principle, could be recycled by pneumatically cleaning it. Combustion power utilized such a technique with a fluidized bed to remove the particulate from the filter media [29]. Recycling of filter media was not desired in this phase of testing, but could be utilized in future testing of the MBGF. Recycling of filter media could greatly reduce the operating costs of the MBGF.

CHAPTER 4: RESULTS AND DISCUSSIONS

Accurate isokinetic sampling of a hot, dirty gas stream proved a major challenge in this research. Problems included gas leaks, the collection of particulate within sample lines, and (apparently) concentration gradients across duct cross-sections. This complicated analysis of moving bed performance, which also experienced some operational difficulties during early stages of performance evaluation, including unstable pressure drops across the MBGF and mass flow problems. Although most of these problems were resolved, reliable isokinetic sampling at elevated temperatures remains a challenge.

Filter media

A non-porous filter media capable of withstanding a high temperature, corrosive environment was desired. Additionally, in order to make the MBGF economic for large scale, long-term operation, an inexpensive filter media must be incorporated. For this reason, something readily available and cheap was desired. This criterion led to American Materials Corp. of Eau Claire, WI. Their relatively dust-free and uniform sized Red Flint gravel, which is commonly used in water treatment and filtration applications, was ideal for the dry scrubbing of gases. Typical chemical compositions can be found in table 1.

Table 1: Filter media chemical composition

Chemical Compound	**% Composition**
Silica (SiO_2)	92.87
Iron Oxide (Fe_2O_3)	3.42
Loss on Ignition (L.O.I.)	1.15
Aluminum Oxide (Al_2O_3)	1.25
Magnesium Oxide (MgO)	0.60
Calcium Oxide (CaO)	0.51
Titanium Dioxide (TiO_2)	0.04
Sodium Oxide (Na_2O)	0.05
Potassium Oxide (K_2O)	0.06
Sulfur Trioxide (SO_3)	0.04
Barium Oxide (BaO)	0.01

Gravel sizes of 4 mm diameters were chosen for testing. As shown by Shi [30], careful selection of granule size is critical to efficient filter performance. If pebbles are too small, they will readily fluidize in the down-comer of the filter at high volumetric flow rates, which appears to increase the penetration of dust through the filter. Furthermore, for "high velocities", granules may become "stationary" against the screen while particles at the bottom of the down-comer become fluidized. The agitation of dust collected at the base might allow it to rise into the down-comer, which will get stalled in a "dead zone" near the exit, resulting from particles flowing down the center in almost a rat-hole phenomena.

The critical conditions for good filter performance is thought to be $U/U_{mf}<1$ where U is the superficial velocity of gas in the riser and U_{mf} is the minimum fluidization velocity of granules used as bed media. Minimum fluidization velocity, U_{mf}, can be approximated by three different equations [31]. For smaller Reynolds numbers, Re<20, U_{mf} can be approximated by:

$$U_{mf} = \frac{(\Psi d_v)^2}{150}\frac{(\rho_p - \rho_g)g}{\mu}\left(\frac{\varepsilon_{mf}^3}{(1-\varepsilon_{mf})}\right) \tag{6}$$

where ψ is the media sphericity, d_v is the volume diameter of media, ρ_p is the media density, ρ_g is the producer gas density, ε_{mf} is the voidage of the filter media at the incipiently fluidized state, and μ is the viscosity of the producer gas. At larger Reynolds numbers, Re>1000, U_{mf} is better approximated by:

$$U_{mf} = \sqrt{\frac{\Psi d_v}{1.75}\frac{(\rho_p - \rho_g)g}{\rho_g}\varepsilon_{mf}^3} \tag{7}$$

A good approximation for the minimum fluidization velocity at any Reynolds number is:

$$U_{mf} = \frac{\mu}{d_v \rho_g}\left[\sqrt{(1135.7 + 0.0408Ar)} - 33.7\right] \tag{8}$$

Implementing the operating conditions during a test and the 4 mm filter media used, equations 6-8 yielded a minimum fluidization velocity of 2.79 m/s. Additionally, the respective velocities during each test can be found in table 2, which is given below.

Table 2: MBGF velocities

Test	Gas Contact Velocity (m/s)	Down-comer Velocity (m/s)
I1-01	1.32	0.51
I1-02	1.53	0.50
I1-03	1.65	0.67
I1-04	1.67	0.66
I2-01	1.5	0.56
I2-02	1.44	0.53
I2-01A	0.46	0.16

Excluding Test I2-01A, the average velocities for the gas contact zone and down-comer were 1.5 m/s and 0.57 m/s, respectively. Both were much lower that the minimum fluidization velocity. But the gas contact region is where the gas impacts the filter media downwardly and is not likely to fluidize. However, the velocities within the down-comer would be likely to fluidize as a result of upward force acting on the filter media. It should be noted that the MBGF did not experience any fluidization during testing.

Alternative filter medias may also be incorporated into the filter such as limestone. It is well know that the injection of limestone in a biomass gasifier can absorb some of the tars. Similar characteristics should be expected if used as a filtering media. Although used in a fixed-bed granular filter, Swift et al. [32] and Johnson [33] determined that acceptable collection efficiencies were found when a limestone sorbent was used. However, it was decided that limestone would not be considered for testing at this time as a result of the potential for the attrition and elutriation of limestone dust into the gas stream.

Operating conditions

Each test performed had specific conditions and variables that helped to compare to other tests. Some of these included the MBGF media removal rate, volumetric flow rate of

gas passing through the MBGF, the steady-state gasifier temperature, and the gasifier fuel rate. These values for each respective test can be found in table 3 given below.

Table 3: Operating conditions and values.

Test	Media Flow Rate (kg/hr)	Volumetric Flow Rate (standard m^3/min)	Gasifier Temperature (C)	Gasifier Fuel Rate (kg/hr)
I1-01	4.4	5.32	732	113*
I1-02	6.6	6.29	732	133*
I1-03	2.2	6.79	732	144*
I1-04	8.7	6.79	732	144*
I2-01	35.3	5.92	815	154
I2-02	69.6	5.96	776	181
I2-01A	35.3	2.10	762	154

*Estimation based on equivalence ratio.

Particulate concentrations

Each test resulted with inlet and exit MBGF concentrations and particulate loading rates. These concentrations can be found in Table 4 below.

Table 4: MBGF Inlet and Exit Particulate Concentrations

Test	Inlet Particulate Concentration (g/m^3)	Inlet Particulate Rate (kg/hr)	Exit Particulate Concentration (g/m^3)	Exit Particulate Rate (kg/hr)
I1-01	60.26	19.25	1.33	0.42
I1-02	29.86	11.26	0.87	0.33
I1-03	29.22	11.90	10.37	4.22
I1-04	29.59	12.05	6.72	2.74
I2-01	2.32	0.82	5.13	1.82
I2-02	2.6	0.94	3.34	1.20
I2-01A	2.09	0.26	2.55	0.32

It should be noted that the gasifier and the sampling system was modified following the Test I1-04. Even though the first four tests presented in Table 4 seem very promising, they were

discredited as a result of small errors in sampling procedure and oxygen leaks. A 5% oxygen leak in the isokinetic sampling system will result in a 25% error in volume of gas sampled. Further problems were encountered in tests I2-01, I2-02, and I2-01A. These problems in addition to the problems found in early testing can be found in a later section with their respective solutions and corrections.

Particulate analysis

Particles collected in the sampling filters were subjected to scanning electron microscopy and energy-dispersive spectroscopy to determine elemental analysis. Scanning electron micrographs of particulate collected at the inlet and exit of the filter were prepared to compare the size of particles at the two locations. Results for Tests I1-01, I1-02, and I2-01 are shown in figures 10 to 12, respectively. As can be seen, there are noticeable differences in particulate size from the MBGF inlet to exit particulate. Figure 10 illustrates the differences in the size distribution between inlet and exit MBGF gas streams. Similarly figures 11 and 12 indicate that the larger particulate was filtered by the MBGF. SEM micrographs show that the average sized dust particle at the inlet is sized at 25 to 30 μm in diameter. At the outlet, there are few particles are as large as 10 μm and most appear to be in the size range of 2 – 3 μm.

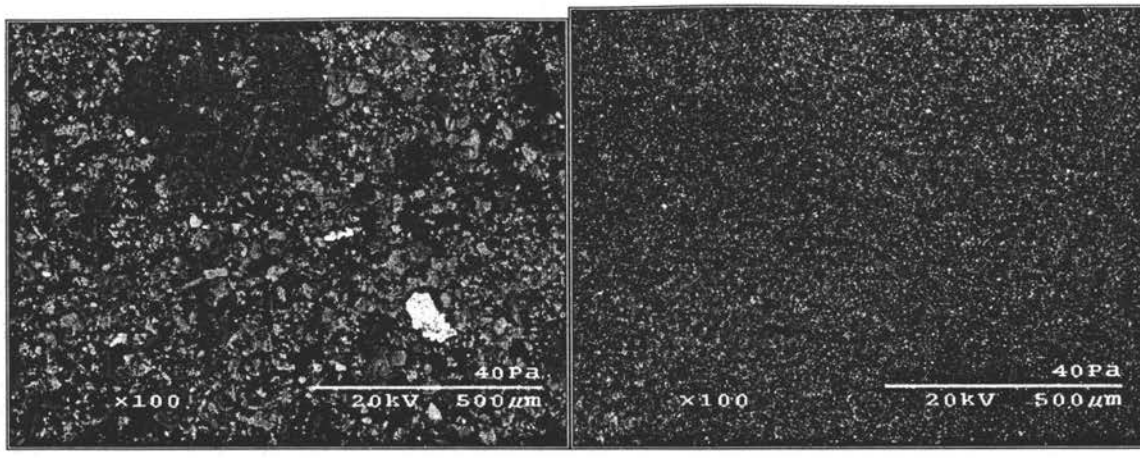

(a) Inlet (b) Exit

Figure 9:Difference in particulate size for Test I1-01 (100x magnification)

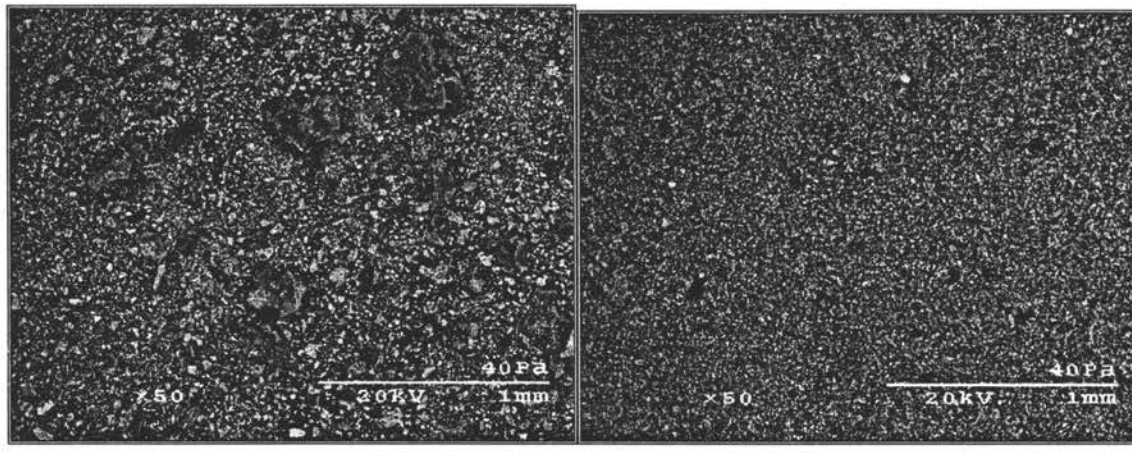

(a) Inlet (b) Exit

Figure 10: Difference in particulate size for Test I1-02 (50x magnification)

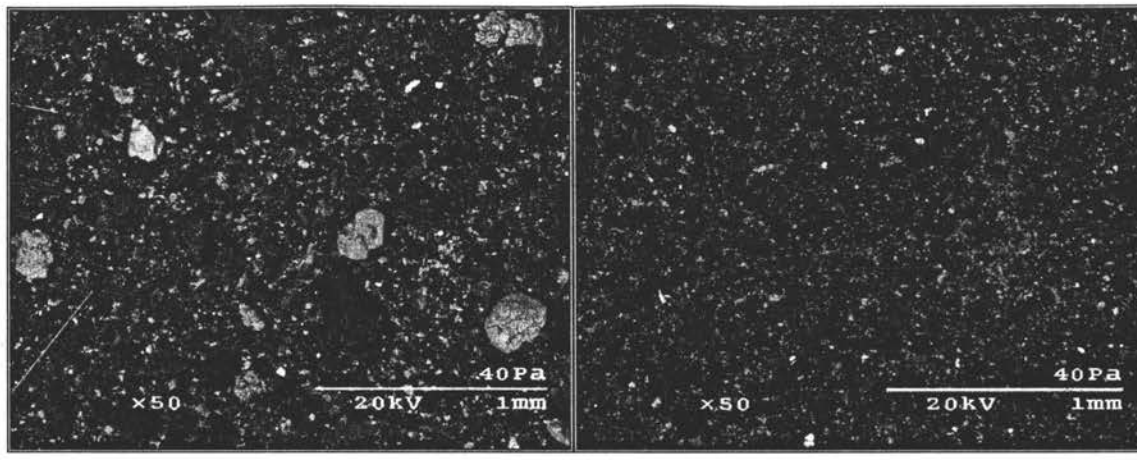

(a) Inlet (b) Exit

Figure 11: Difference in particulate size for Test I2-01 (50x magnification)

Differences in particulate size can be attributed to the proper formation of the dust cake and the vigorous travel path a single particle endures while passing through the MBGF. Assuming an inlet particulate loading rate of 11 kg/hr for Tests I1-01, I1-02, and I2-01; one can compare this value to the media flow rates for these tests, respectively, in Table 2. This comparison shows that the media flow rate for each test is close to the assumed inlet particulate concentration, which enables the MBGF to operate in a steady state and for the proper formation of a dust cake.

Additional particulate from Test I2-02 was analyzed under the SEM, which is shown below in figure 12. Unlike figures 9-11, figure 12 indicates that the MBGF allowed some of the large particulate to pass through. Large particulate, 100 to 300 micron, in size was collected in the MBGF exit.

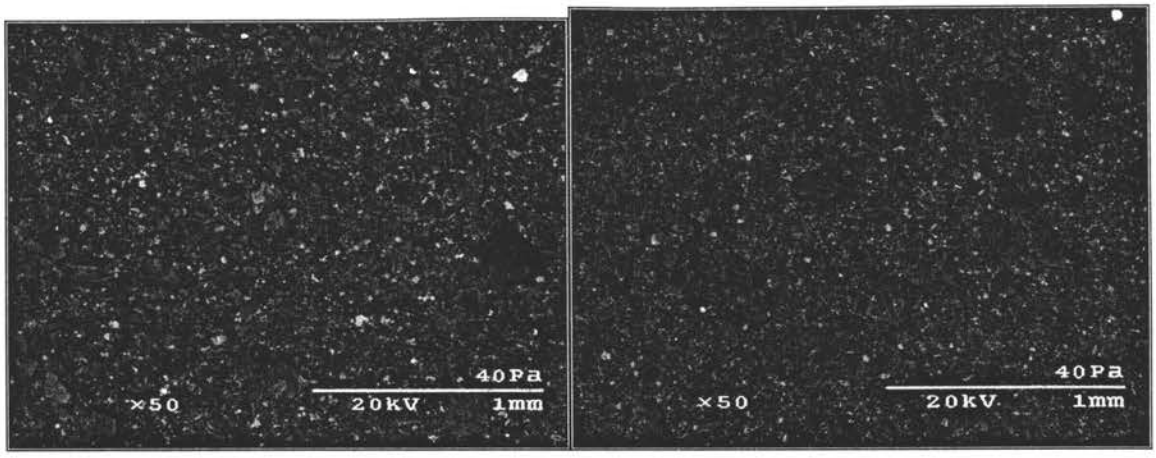

(a) Inlet (b) Exit

Figure 12: Difference in particulate size for Test I2-02 (50x magnification)

Large particulate in the exit stream is non-typical and is not desired. This is indicative of a lack of filtration and/or a lack of proper operation, which may have resulted in bypassing. Assuming an inlet particulate concentration of 11 kg/hr again, it is hypothesized that the high media flow rate of Test I2-02 (69.6 kg/hr), which was six times higher than assumed inlet particulate concentration. This method of operation is thought to have contributed to a poorly formed dust cake at the gas contact region.

Elemental analyses of the inlet and exit streams to the MBGF were also performed and show no dramatic change in dust composition. These graphs can also be found in Appendix C. Of particular significance in the elemental analysis is the absence of silicon enrichment in the particulate at the exit, which might be expected if the silica pebbles were releasing fine dust to the gas stream as it passed through the filter. Granular media must be dust-free and non-friable to be effective in the MBGF. There were no notable and repeatable differences in the spectral analysis.

Furthermore an ATM Model L3P Sonic Sifter was used to get size distributions of dust entering the MBGF on the inlet particulate gathered from Test I1-02. This test was used

to verify the values found by scanning electron microscope, in which they were found to agree closely. The average size of the inlet dust particles was 26.1 μm. As a result of the great amount of time required to perform a sifting analysis on each test, this test was only performed as a means of verification when the data was suspect.

Producer gas composition

During each test, the producer gas was passed to gas chromatography (GC). The GC, which identifies gas compositions, instilled additional confidence in the results and gave an indication that producer gas was actually being drawn. Typical gas compositions of raw producer gas entering the MBGF can be found for each test in Table 5.

Table 5: Raw Producer Gas Composition

Gas Composition	I1-01	I1-02	I1-03	I1-04	I2-01	I2-02	I2-01A
Hydrogen	11.70	7.27	7.32	5.8	6.2	4.9	8.1
Oxygen	0.00	0.18	0.35	0.08	1.4	0.0	0.1
Nitrogen	50.42	51.63	48.83	48.4	49.7	52.7	52.6
Methane	4.44	3.77	4.04	3.8	3.1	3.0	3.8
Carbon Monoxide	10.19	8.86	12.60	12.3	10.2	11.6	13.8
Carbon Dioxide	14.82	16.24	16.90	13.8	13.9	14.9	14.0
Ethylene	2.81	2.85	2.03	1.7	1.7	1.6	1.8
Other	5.62	9.2	7.93	14.12	13.8	11.3	5.8

Since the GC is not calibrated for all gases there are certain gases, probably light hydrocarbons, which are unknown.

Tar concentrations

Testing was also performed that determined the tar concentrations of the producer gas entering and exiting the MBG F following Test I2-01A. The producer gas was allowed to

pass through the series of glass impingers that contained glass beads and the solvent, DCM. The vapor phase tars were condensed from the producer gas stream in these cooled impingers and were suspect to distillation. The tar-loaded solvent was then distilled at 75 °C to determine the amount of heavy tars. Heavy tars were defined to be the residue left over after distilling at 75 °C. The resulting tar concentrations are shown in Table 6.

Table 6: Tar Concentrations for MBGF Inlet and Exit Gas

	Total Heavy Tar (g)	**Standard Gas Volume Sampled (Liters)**	**Heavy Tar Concentration (g/m^3)**
MBGF Inlet	3.63	251.3	14.5
MBGF Exit	4.44	295.0	15.1

As it can be seen, there is not a large difference in tar concentrations between the inlet and exit gas. This indicated that the filter operated at high enough temperatures to prevent condensation of tar. Also, the use of non-porous filter media prevented absorption of tar.

Waste media analysis

Following a test a representative sample of the dirty filtering media was drawn from the waste collection barrel. A sample of clean filter media was also taken, in which both samples were sifted using a Row Tap sifter. Utilizing a series of sifting screen a size distribution was attained. A small percentage of mass in the dirty filter media can be attributed to particulate as well as a small percentage of mass in the clean media can be attributed to silicon dust. The difference in the dirty filter media (i.e. particulate and silicon dust) and the clean filter media (i.e. silicon dust) led to a percentage of mass attributed to particulate. Through this test it was found that 2.4 % of the waste media sampled was attributed to particulate.

The large amount of time required for a pebble to travel from the gas contact region to the waste barrel or residence time can create some difficulty in assigning the results to a specific test. However, the waste media analysis followed Test I2-02 whose length was much greater than the residence time of granules in the filter. Specifically, the residence time for the test was 3.05 hours and the filter media was being removed at a rate of 68.04 kg/hr (150 lb/hr) for approximately 5.14 hours. The waste media analysis represented the final 2 hours of the 5.14-hour test.

Utilizing the volumetric flow rate of the gas flowing through the MBGF, which was 5.96 standard m^3/min (210 standard ft^3/min), the moving bed filter collected about 4.6 g/m^3 of dust entering the filter, which is the same order of magnitude as measured isokinetically for the last several experimental trials. This result illustrates that the filter is removing a substantial quantity of dust. Nevertheless, this result also shows that isokinetic sampling is in error, as a mass closure on dust entering and leaving the filter cannot be performed.

Shortcomings and improvements

During preliminary testing, fluctuating pressure drops were observed across the filter after about 1 hour of operation. Graphs of the unsteady and fluctuating pressure drops can be seen in figures 13-16 shown below.

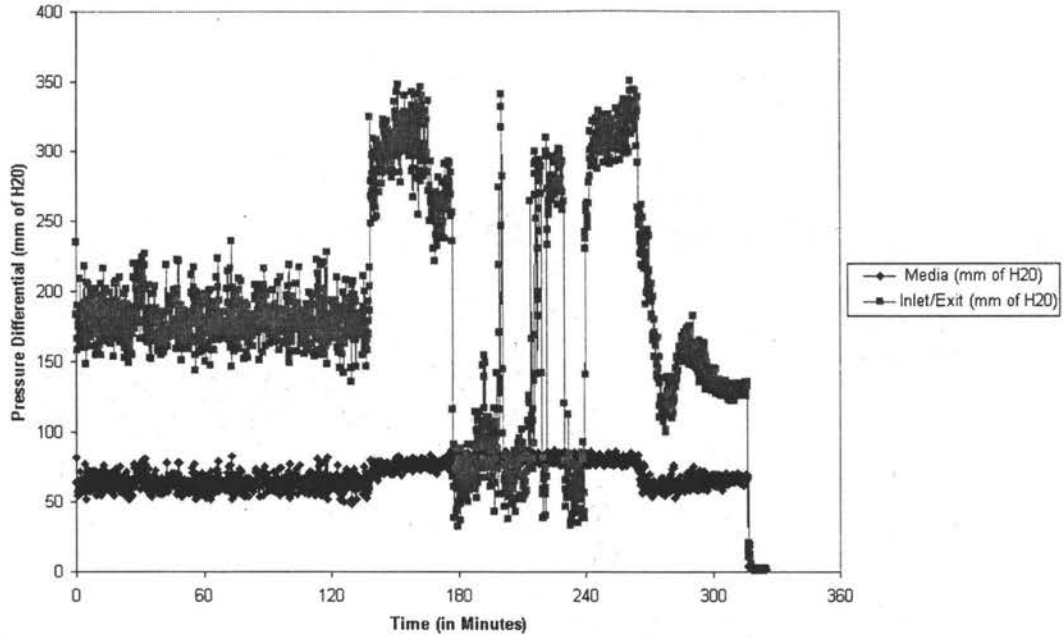

Figure 13: MBGF Pressure Drop Data (Test I1-01)

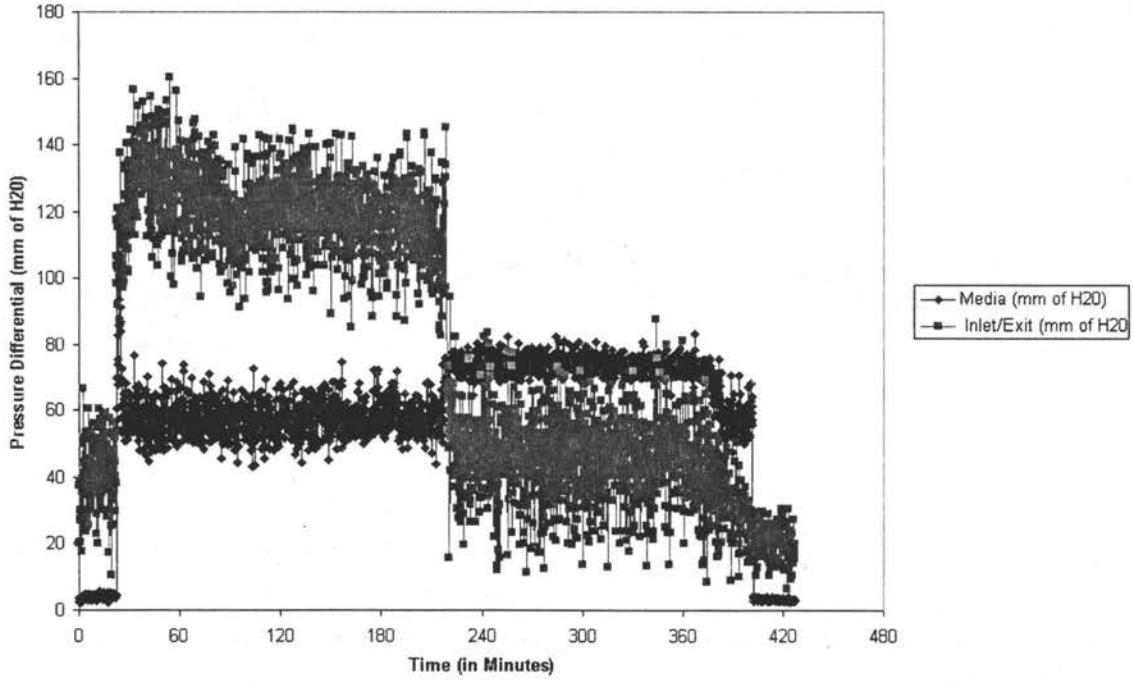

Figure 14: MBGF Pressure Drop Data (Test I1-02)

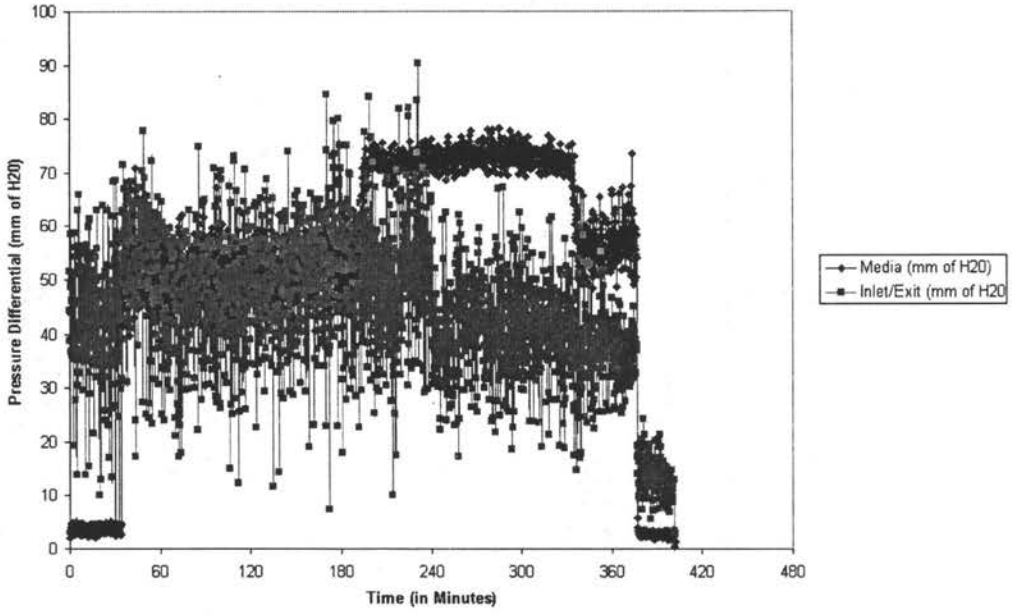

Figure 15: MBGF Pressure Drop Data (Test I1-03)

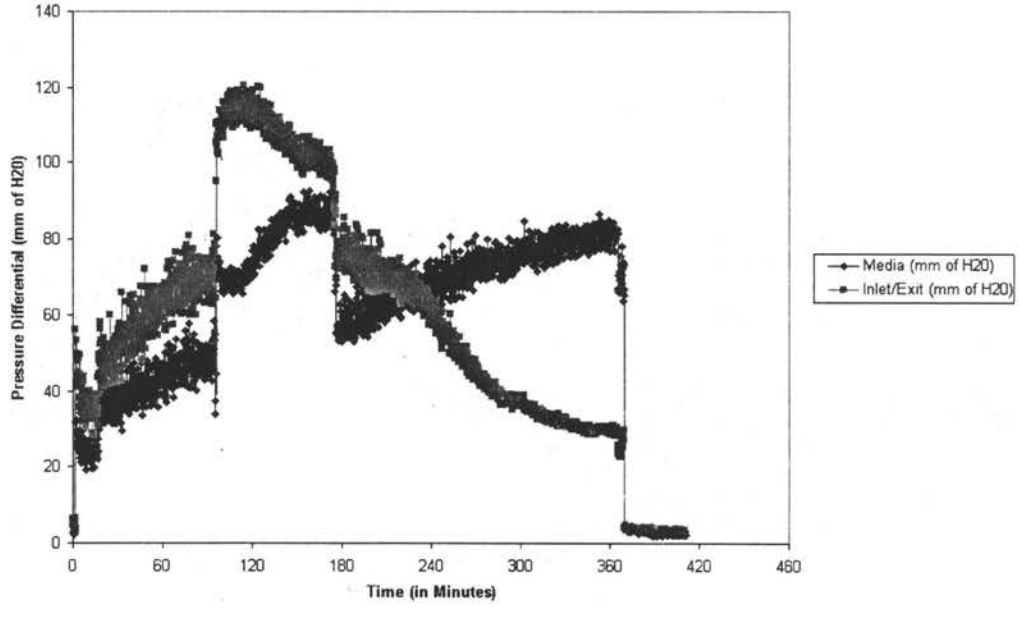

Figure 16: MBGF Pressure Drop Data (Test I1-04)

While figures 13 -16 show erratic pressure drops across the MBGF, figures 17 and 18 show steady pressure drops across the MBGF. It should be noted that all pressure drop graphs include the start-up of the MBGF and only the last section (2-3 hours) of the graph represent actual isokinetic sampling. This change is the result of the installation of a double-cone insert. This insert will be given more detail later in this section.

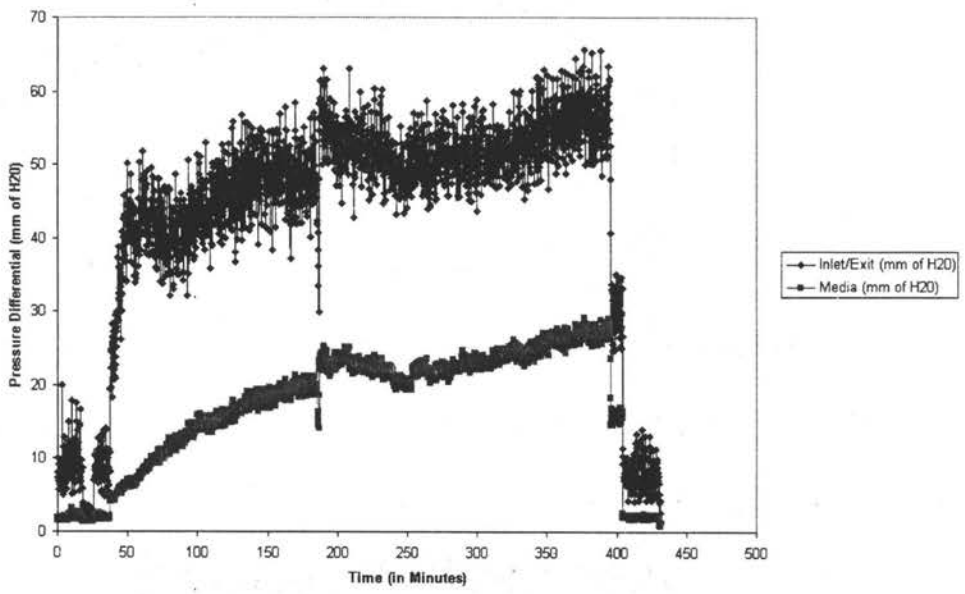

Figure 17: MBGF Pressure Drop Data (Test I2-01)

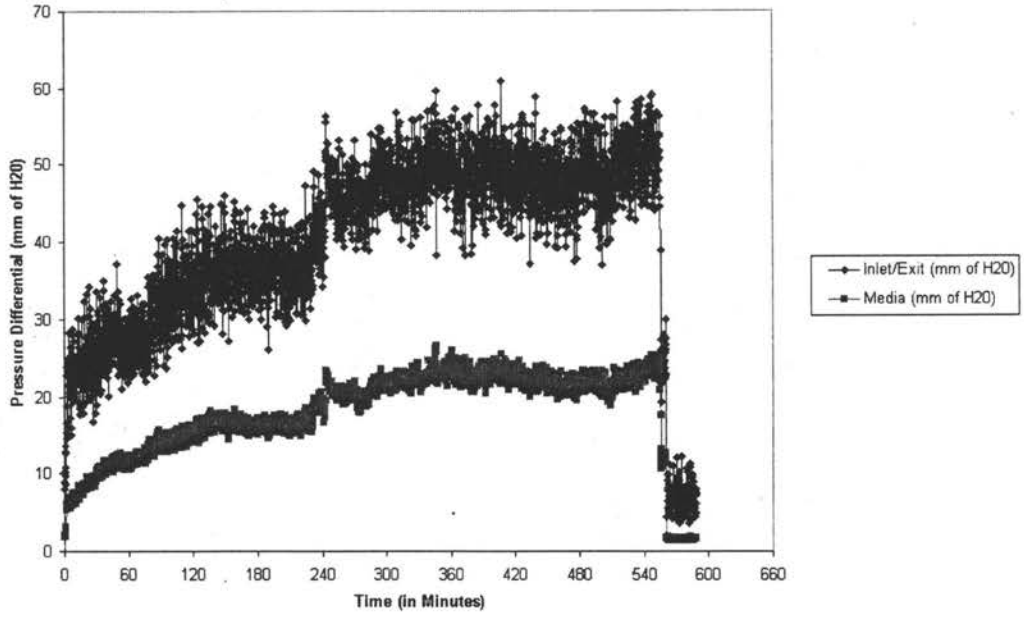

Figure 18: MBGF Pressure Drop Data (Test I2-02)

However, the cause of the erratic pressure fluctuations was not known initially. Not until an inspection of the MBGF did it became apparent that roughly 75% of the flow straightening fins were plugged with dust. This Figure 19 illustrates plugging of the fins.

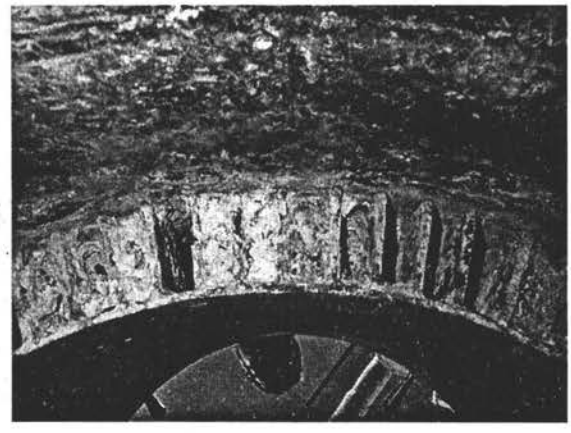

Figure 19: Plugged Flow Straighteners

The plugging resulted from a lack of proper operation of the MBGF, which included non-steady-state operation and non-mass flow of filter media.

As introduced in a previous section, the media flow rate of the filter needs to be as close to the entering particulate loading rate for proper operation of the filter. However, it should not be lower than this value. This condition will result in a non-steady state operation. Essentially, there would be more mass entering the filter than exiting. This can result in plugging and reduced operation of the filter. However, following this discovery the media flow rate was increased to exceed the entering particulate loading rates. A dust-to-pebble ratio was also introduced to help characterize this relationship, which can be found below.

$$\text{Dust - to - Pebble Ratio} = \left(\frac{\text{Inlet Dust Concentration} \left(\frac{kg}{hr} \right) \times \text{Efficiency}}{\text{Granular Flow Rate} \left(\frac{kg}{hr} \right)} \right) \times 100$$

Likewise, it could be expected that a higher dust-to-pebble ratio is more desirable. This is easily controlled by the granular flow rate. Furthermore, lower granular flow rates result in decreased material handling, which ultimately reduces operational costs and maintenance of the overall system.

Another design parameter of the MBGF was the mass flow of media flowing through the filter. Mass flow is simply a condition in which all media within the filter travels downward at the same velocity. This condition is better illustrated in figure 20.

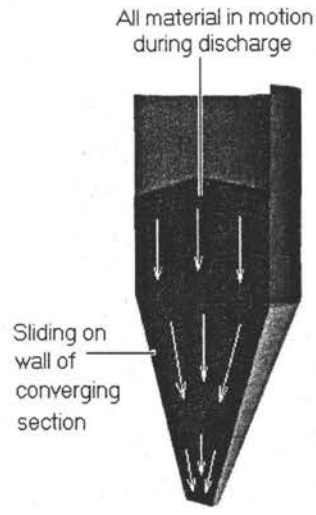

Figure 20: Mass flow schematic [34]

However, there are some operational problems that could be encountered. One includes rat holing, which is defined as a single channel located at the center of the filter where media flows downwardly at velocities much higher that the media at the walls. Therefore creating a funnel-like appearance, which is illustrated in figure 21.

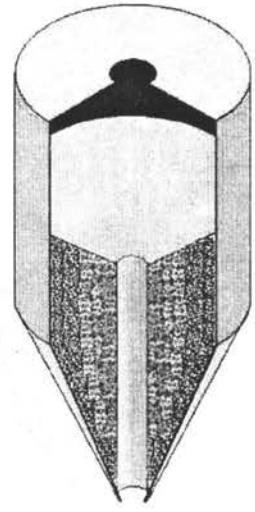

Figure 21: Rat holing schematic [34]

Tests were performed on the MBGF media to determine if rat holing occurred. This test consisted of painting concentric circles on a level media surface while removing the media at a constant rate for a prolonged period of time. After a few hours the inner circles were consumed, which clearly demonstrated rat holing. This test is illustrated in figure 22.

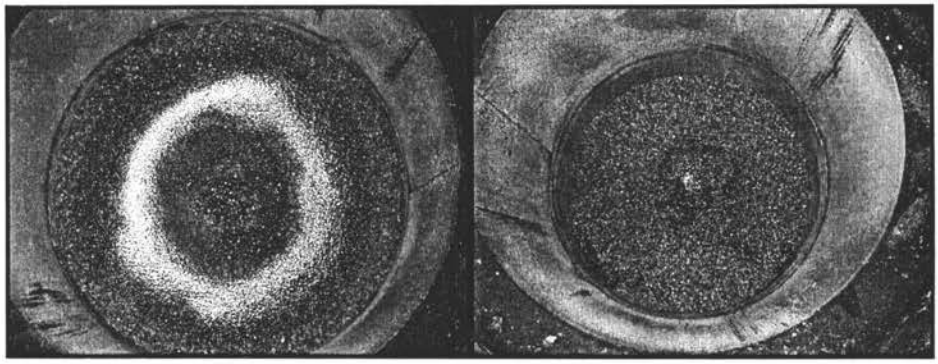

a) Before b) After

Figure 22: Rat holing test

Through this it was discovered that rat holing was occurring in the filter. From this condition it could be assumed that the filter media at the gas contact region was not being replaced in a steady-state manner. Tests I1-01, I1-02, I1-03, and I1-04 are all suspected of rat holing. Therefore, the media was saturated with incoming dirty gas, which led to the formation of a dust cake without being continuously covered by a clean layer of granular material.

The problem of rat holing was fixed by including an insert where the channeling was occurring. The same test performed in the previous paragraph was performed to verify mass flow. Figure 5 illustrates the double-cone insert within the MBGF while a picture of the double-cone insert is shown in figure 23.

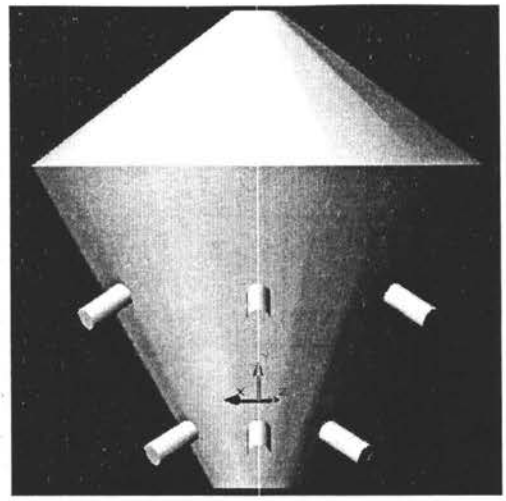

Figure 23: Schematic of the MBGF with the Double-cone insert.

Other problems encountered during testing dealt around isokinetic sampling at high temperatures. Throughout every test there were concerns about oxygen leaks. Producer gas should have no oxygen. Oxygen within slipstreams was indicative of a leak within the sample line, which could skew the results. Therefore it was mandatory to verify that the sample lines were leak free. This was done via a Micro GC, which could accurately determine oxygen levels down to fractional levels. The first five tests had an oxygen leak on one or both of the lines. Not until the last four tests did the sample lines have no leaks. Attaining leak free lines required great detail during installation to insure an oxygen free environment.

Similarly, there were problems with the initial particulate filter that was used on the downstream side of the MBGF. This sample line employed a Mott 6300 Series sintered metal filter, which consisted of 7 individual porous cups filter utilized a carbon fiber gasket. This filter was employed because of its lower weight, which could help increase the measurement of small changes in mass. However, during testing it was found that the porous cups would plug with particulate, thus not accurately measuring the amount of particulate

sampled. Additionally, the carbon fiber gasket was found to be very friable after sustaining high temperatures of 450 °C (842 °F) for prolonged periods of time. Another drawback of this type of filter was the pressure drop that the gas experienced. This had negative effects on the pump performance and load.

An initial attempt to correct the plugging led to the reversal of the porous cups, which allowed the particulate to collect in the filter housing. This correction enabled the filter to collect additional particulate, but difficulties in comparing dissimilar sample lines, oxygen leaks, and dismantling the porous cup particulate filter led to the installation of the same filter used in the MBGF inlet sample line.

After all of these changes where made in addition to the upgrades to the gasifier and its exhaust, a series of testing followed. Obtaining reproducible results was never attained from one test to the next. In fact the second series of tests, negative filter efficiencies were indicated, clearly an impossible situation except if the filter itself was generating large amounts of dust. Analysis of the waste filter media and SEM microforms indicate that this was not the case.

It is hypothesized that particulate concentration gradients exist within the cross section of the exhaust pipes, which led to gross sampling errors. Obtaining traverses of the duct in order to determine whether concentration gradients existed is extremely difficult and were not attempted in this study. It should be the subject of a future study.

Through this series of testing many things have been learned. For example, it has been discovered that a filter media that retards fluidization is desired for higher collection efficiencies. Particulate captured in the sintered metal filter for the MBGF inlet and exit streams ranged from 20 to 25 micron and 2 to 3 micron, respectively. Analysis of this

particulate indicates that there are no obvious differences in chemical composition. Typical gas compositions from the biomass gasifier have been established for base comparisons. Likewise, tar concentrations have been determined, in which it shows that the current filter media used in the MBGF does not condense tar. All of these things have led to a better understanding to the operation of the MBGF and isokinetic sampling.

CHAPTER 5: CONCLUSIONS AND RECOMMENDATIONS

As a result of problems in high temperature isokinetic sampling, the efficiency of the MBGF was not accurately determined. However, it appears that the inlet concentration to the MBGF was in the range of 2 to 30 g/m^3, with the most likely level being around 5 g/m^3. There are several clues that indicate that the MBGF was working at relatively high efficiency, although this could not be quantified. Particulate analysis under the scanning electron microscope (SEM) showed no traces of silicon, a major component of the filter media, which disproved a concern that the MBGF was adding dust from the granular media to the producer gas stream. The SEM results also showed that the MBGF effectively removed most of the largest particulate from the entering gas stream, which suggests filtration to some degree. Additionally, an analysis of the waste MBGF filter media showed that up to 5 g/m^3 of dust was being removed from the entering stream. All of these results point toward a reasonable level of filtration.

Future Work

Areas of improvement lie within the isokinetic sampling system and mass accounting. Specifically, one of the major assumptions made before sampling commenced, which needs to be confirmed, was that the flow profile had a uniform velocity profile and a uniform particulate concentration gradient across the exhaust duct. Tests confirm that the flow profile had a uniform velocity distribution, but no data has been collected that supports the claim of uniform dust loading. A non-uniform particulate concentration gradient across the duct can cause significant variation in calculated particulate concentration, thus leading to errors in collection efficiency.

Before any further testing commences a determination needs to be made on the presence or absence of radial concentration profiles. This test would inject a known amount of particulate into the gasifier with a known volumetric flow of air while operating at cold temperatures. Atmospheric temperatures would allow for a less complicated set-up and would reduce the chances for failure. The procedure for this test may include collecting particulate in a paper filter in various locations across the exhaust duct. This procedure would be similar to the log-Tchebycheff rule or the equal area method used in determining the velocity profile, which was discussed briefly in a previous section. This test would strengthen the assumption of a uniform dust loading across the duct while giving additional confidence in the location of the sample probes.

Another area that could use improvement is performing mass balances. This has not been implemented into the system because of the difficulties in material handling. The size of the MBGF, its reservoir, and the large volume of filtering media make it hard to perform a mass balance on the entire system. The method of warming up the MBGF while in combustion mode also adds difficulty since this period typically takes 2-4 hours. The MBGF actually only experiences gasification during the length of a test and the time required attaining a steady state pressure drop. In future testing one may remove all filtering media at the end of a test. Despite its difficulties the information gained may prove very valuable. A mass balance could reinforce data collected in the isokinetic sample lines.

As a result of the complications experienced in high temperature isokinetic sampling, a few variables were never tested. However, these variables still need to be tested so that a full assessment of the MBGF can be made. Specifically, an understanding of the effect of filter media size, depth of filter media, and flow rates on the overall pressure drop and

collection efficiency of the MBGF is needed. This information will lead to a better understanding of moving bed granular filters and will aid in future moving bed granular filter designs.

REFERENCES

1. Tsubaki, J. and Tien, C., "Gas Filtration in Moving Beds: An Experimental Study." The Canadian Journal of Chemical Engineering, Vol. 66, April 1988, Pages 271-275.
2. Kuo, J.T., Smid, J., Hsiau, S.S., and Chou, C.S. "Granular Bed Filter Technology." Proceedings of the National Science Council, Republic of China, Part A: Physical Science and Engineering, v 22, n 1, Jan. 1998, Pages 17-34.
3. Hinds, William C., Aerosol Technology: Properties, Behavior, and Measurement of Airborne Particles, 2nd Ed., Wiley-Interscience Publication, 1999.
4. Reijnen, K. and Van Brakel, J. "Gas cleaning at high temperatures and high pressures: A review." Powder Technology, Vol. 40, Issues 1-3, October-December 1984, Pages 81-111.
5. Spurny, Kvestoslav, Advances in Aerosol Filtration, Lewis Publishers, 1998.
6. Schulz, Karsten. Permission to use figure from Herding GmbH Filtertechnik, April 2002.
7. EPA-CICA Fact Sheet, Fabric Filters: Reverse Air-Cleaned Type.
8. Donovan, R.P., Fabric Filtration for Combustion Sources, Marcel Dekker, Inc., 1985
9. Dickenson, T. Christopher, Filters and Filtration Handbook, 4th Ed, Elsevier Advanced Technology, Oxford, U.K., 1997.
10. Ogawa, Akira. Separation of Particluates from Air and Gases, Vol. 2, 1984.
11. Phil Decker, Permission to use figure from Powerspan Corporation, April 2002.
12. EPA Air Pollution Technology Fact Sheet for Dry Electrostatic Precipitators. Web Site: http://www.epa.gov/ttn/catc/dir1/fdespwpl.pdf, Access July 17, 2002.

13. Reijnen, K. and Van Brakel, J. "Gas cleaning at high temperatures and high pressures: A review." Powder Technology, Vol. 40, Issues 1-3, October-December 1984, Pages 81-111.

14. Reijnen, K. and Van Brakel , J. "Gas cleaning at high temperatures and high pressures: A review." Powder Technology, Vol. 40, Issues 1-3, October-December 1984, Pages 81-111.

15. Squires, A.M. & Pfeffer, R., "Panel bed filters for simultaneous removal of fly ash and sulfur dioxide: 1. Introduction." J. Air Pollution Control Assoc. 20, 1970, 534-538.

16. Lipert, T. E. et al. "Testing and verification of granular bed filters for removal of particulates and alkalies: High Temperature, High Pressure Particulate and Alkali Control in Coal Combustion Process Streams." Proceedings U.S. DOE Contractors' Meeting, CONF-810249, 1981, Pages 471-489.

17. Hall, H. J. and Munday, J.C., "Purification of gases." U.S. Patent 2,411,208, 1946.

18. Dorfan M. I., "Method and apparatus for suppressing steam and dust rising from coke being quenched." U.S. Patent 2,604,187, 1952.

19. Saxena, S. C. et al., "Particulate removal from high temperature, high pressure combustion gases", Prog. Energy Combust. Sci. 11, 1985, Pages 193-251.

20. Guillory, J. L., "High-Temperature Moving Bed Granular Filter Development at Combustion Power Development Company." Third Annual Contaminant Control in Hot Coal Derived Gas Streams, Contractors' Meeting Proceedings, 1983, Pages 245-269.

21. Brown, R. C., Smeenk, J., and Wistrom, C., "Design of a moving bed granular filter for biomass gasification." Proceedings of the Progress in Thermochemical Biomass Conversion Conference, Tyrol, Austria, September 17-22, 2000.

22. Smeenk, J. and Brown, R. C., "Experience with atmospheric fluidized bed gasification of switchgrass." BioEnergy '98 Conference, Madison, WI, October 4-8, 1998.

23. Hinds, William C., Aerosol Technology: Properties, Behavior, and Measurement of Airborne Particles, 2nd Ed., Wiley-Interscience Publication, 1999.

24. Mudry, R., Permission to use figure from Air Flow Science, June 2002.

25. Pitot-Static Tubes Method. ASHRAE Handbook: Fundamentals, 2001.

26. Albrecht, J., Deutsch, S., Kurkela, E., Simell, P., Sjostrom, K., "Provisional Protocol For The Sampling And Analysis of Tar and Particulates In The Gas From Large-Scale Biomass Gasifiers. Prepared by a working group of the biomass gasification task of the IEA Bioenergy Agreement." 1998.

27. Measuring Flow in Ducts. ASHRAE Handbook: Fundamentals, 2001.

28. Incropera, F. and DeWitt, D., Fundamentals of Heat and Mass Transfer, 4th Ed, 1996.

29. Guillory, J. L., "High-Temperature Moving Bed Granular Filter Development at Combustion Power Development Company." Third Annual Contaminant Control in Hot Coal Derived Gas Streams, Contractors' Meeting Proceedings, 1983, Pages 245-269.

30. Shi, Huawei, Masters Thesis, Similitude modeling and experiments on a moving bed granular filter. Iowa State University, 2002.

31. Kunni, D. and Levenspiel, O., Fluidization Engineering, 2nd Ed, Butterworth-Heinemann series in chemical engineering, 1991.

32. Swift, W. M., et al. "Plans and studies on flue gas cleaning and particulate monitoring in PFBC." Proceedings from the 5th International Conference on FBC, Vol. II, Near Term Implementation, M78-68, Dec. 1978, Pages 493-521.

33. Johnson, I., et al., "Gas Cleaning and emission control for pressurized combustion.", CONF-7906157, Pages 186-210.

34. Farnish, Richard, permission to use figure from the Wolfson Centre for Bulk Solids Handling Technology, University of Greenwich, July 2002.

APPENDIX A

Pre and Post MBGF Isokinetic Sample Line Flow Calculations

Andy Suby
Jerod Smeenk
4/24/01

Properties of air at standard temperature and pressure:

$T_{stan} = 298.15K$ Temperature of air at standard conditions

$P_{stan} = 14.696psi$ Pressure of air at standard conditions

$\rho_{stan\_air} := \rho(T_{stan}, P_{stan})$

$\rho_{stan\_air} = 0.074 \frac{lb}{ft^3}$ Density of air at standard conditions

At pitot tube sampling point downstream of the MBGF:
(PG = Producer Gas)

$T_{PGPitot2} := (441 + C\_K) \cdot K$

$T_{PGPitot2} = 714K$ Approx. temperature of the PG

$P_{PGPitot2} := P_{stan} + \frac{1.5}{27.71} \cdot psi$

$P_{PGPitot2} = 14.75psi$ *Approx. pressure of the PG

$\rho_{PGPitot2} := \rho(T_{PGPitot2}, P_{PGPitot2})$

$\rho_{PGPitot2} = 0.031 \frac{lb}{ft^3}$ *Approx. density of the PG

Flow Determination:

ΔP measured with s-pitot tube (Units adjusted from in. w.c. to match ASHRAE)

$\Delta P_2 := .25 \cdot \frac{lbf}{ft^2}$

$C := 136.8$ Unit conversion factor

$CF := 1.5$ s-pitot tube correction factor

$gc := 32.174 \frac{lb \cdot ft}{lbf \cdot min^2}$ gravity (units adjusted)

$$V_{PGPitot2} := C \cdot \left[\frac{2 \cdot \left(\frac{\Delta P_2}{CF} \right) \cdot gc}{\rho_{PGPitot2}} \right]^{0.5}$$

$V_{PGPitot2} = 2.545 \times 10^3 \frac{ft}{min}$ Measured Velocity

$D_{prod} := 5.75 in$ Diameter of producer gas duct

$$A_{PG} := \frac{\pi \cdot (D_{prod})^2}{4}$$

$A_{PG} = 0.18 ft^2$ Cross sectional area of producer gas duct

$Q_{PGPitot2} := V_{PGPitot2} \cdot (A_{PG})$

$Q_{PGPitot2} = 458.96 \frac{ft^3}{min}$ Average PG volumetric flow rate

Flow through the MBGF

$Q_{PGPitot} := Q_{PGPitot2} - Q_{PGPitot1}$

$Q_{PGPitot} = 175.517 \frac{ft^3}{min}$

For Sample Line downstream of MBGF:
(PG = Producer Gas)

$T_{PGPost} := (450 + C\_K) \cdot K$

$T_{PGPost} = 723 K$ Approx. temperature of the PG

$P_{PGPost} := P_{stan} + \frac{2}{27.71} \cdot psi$

$P_{PGPost} = 14.768 psi$ *Approx. pressure of the PG

$\rho_{PGPost} := \rho(T_{PGPost}, P_{PGPost})$

$\rho_{PGPost} = 0.031 \frac{lb}{ft^3}$ *Approx. density of the PG

$D_{samp} := .1175 in$ Diameter of sample tube

$$A_{samp} := \frac{\pi \cdot (D_{samp})^2}{4}$$

$A_{samp} = 7.53 \times 10^{-5}\ ft^2$ Cross-sectional area of sample tube

Figure 1 below illustrates the Producer Gas sampling system configuration.

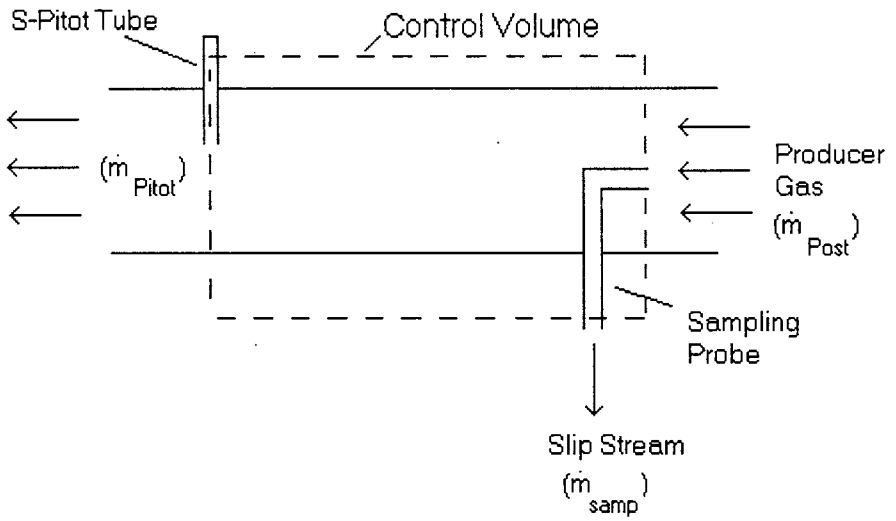

Figure 1.

Due to the conservation of mass, the necessary rotometer flow rate can be determined by the following methodology:

$$\dot{m}_{Post} = \dot{m}_{samp} + \dot{m}_{Pitot}$$

Substitution yields:

$$\rho_{PGPost} \cdot Q_{PGPost} = \rho_{PGsamp} \cdot Q_{PGsamp} + \rho_{PGPitot} \cdot Q_{PGPitot}$$

Or

$$\rho_{PGPost} \cdot V_{PGPost} \cdot A_{PG} = \rho_{PGsamp} \cdot V_{PGsamp} \cdot A_{samp} + \rho_{PGPitot} \cdot Q_{PGPitot}$$

*Approximating producer gas to have similar properties to air

Rearranging and assuming $\rho_{PGPost} = \rho_{PGsamp}$ and $V_{PGPost} = V_{PGsamp}$ for isokinetic sampling:

$$V_{PGPost} := \frac{\rho_{PGPitot2} \cdot Q_{PGPitot}}{\rho_{PGPost} \cdot (A_{PG} - A_{samp})}$$

$$V_{PGPost} = 984.797 \frac{ft}{min}$$

$$Q_{SampPost} := V_{PGPost} \cdot A_{samp}$$

$Q_{SampPost} = 1.236 \times 10^{-3} \frac{ft^3}{sec}$ Volumetric flow rate of sample tube

$Q_{RotoPost} := Q_{SampPost} \cdot \frac{\rho_{PGPost}}{\rho_{stan\_air}}$

$Q_{RotoPost} = 0.87 \frac{liter}{min}$ Flow rate for downstream sample location

At sampling point upstream of the MBGF:
(PG = Producer Gas)

$T_{PGPre} := (594 + C\_K) \cdot K$

$T_{PGPre} = 867K$ Approx. temperature of the producer gas

$P_{PGPre} := P_{stan} + \frac{4}{27.71} \cdot psi$

$P_{PGPre} = 14.841psi$ Approx. pressure of the producer gas

$\rho_{PGPre} := \rho(T_{PGPre}, P_{PGPre})$

$\rho_{PGPre} = 0.025672 \frac{lb}{ft^3}$ Approx. density of the producer gas

Flow determination:
By the same methodolgy as above:

$V_{PGPre} := \frac{\rho_{PGPost} \cdot V_{PGPost} \cdot A_{PG}}{\rho_{PGPre} \cdot (A_{PG} - A_{samp})}$

$V_{PGPre} = 1.176 \times 10^{3} \frac{ft}{min}$ Average velocity of producer gas

$Q_{SampPre} := V_{PGPre} \cdot A_{samp}$

$Q_{SampPre} = 1.476 \times 10^{-3} \frac{ft^3}{sec}$ Volumetric flow rate of sample tube

$Q_{RotoPre} := Q_{SampPre} \cdot \frac{\rho_{PGPre}}{\rho_{stan\_air}}$

$$Q_{RotoPre} = 0.871\frac{liter}{min}$$

Flow rate for upstream sample location

$$Q_{PGPost} := \frac{\rho_{PGPitot2} \cdot Q_{PGPitot} + \rho_{PGPost} \cdot Q_{SampPost}}{\rho_{PGPost}}$$

$$Q_{PGPost} = 177.587\frac{ft^3}{min}$$

$$Q_{PostStand\_air} := \frac{\rho_{PGPost} \cdot Q_{PGPost}}{\rho_{stan\_air}}$$

$$Q_{PostStand\_air} = 73.593\frac{ft^3}{min}$$

Standard Volumetric Flow rate through MBGF

$$Q_{PGPre} := \frac{\rho_{PGPost} \cdot Q_{PGPost} + \rho_{PGPre} \cdot Q_{SampPre}}{\rho_{PGPre}}$$

$$Q_{PGPre} = 212.009\frac{ft^3}{min}$$

$$Q_{Prestand\_air} := \frac{\rho_{PGPre} \cdot Q_{PGPre}}{\rho_{stan\_air}}$$

$$Q_{Prestand\_air} = 73.623\frac{ft^3}{min}$$

Constants

Gas Constant for Air:

$F\_R \equiv 459.67$

Conversion from F to R

$R\_F \equiv -459.67$

$C\_K \equiv 273$

Conversion from C to K

$K\_C := -273$

$inH2O\_psi \equiv 27.71^{-1}$

Conversion from in H2O to psi

$psi\_inH2O \equiv 27.71$

$$R_{air} \equiv \frac{8.314\frac{joule}{mole \cdot K}}{28.97\frac{gm}{mole}}$$

$P_{stan} \equiv 1 \cdot atm$

Atm pressure:

$T_{stan} \equiv (77 + F\_R) \cdot R$

STP temperature

Empirical constants for air Cp calcs (Shapiro):

$\alpha \equiv 3.653$

$\beta \equiv -0.7428$

$\gamma \equiv 1.017$

$\delta \equiv -0.328$

$\varepsilon \equiv 0.02632$

$$Cp(T) \equiv R_{air}\cdot\left[\alpha + \left(\beta\cdot 10^{-3}\right)\cdot\left(\frac{T}{R}\right) + \left(\gamma\cdot 10^{-6}\right)\cdot\left(\frac{T}{R}\right)^2 + \left(\delta\cdot 10^{-9}\right)\cdot\left(\frac{T}{R}\right)^3 + \left(\varepsilon\cdot 10^{-12}\right)\cdot\left(\frac{T}{R}\right)^4\right]$$

Ideal gas relations:

$$\rho(T,P) \equiv \frac{P}{R_{air}\cdot T}$$

Viscosity relations (air):

$$\mu(T) \equiv \left[52.584 + 0.262\left(\frac{T}{R}\right) - 2.954\,10^{-5}\cdot\left(\frac{T}{R}\right)^2\right]\cdot 10^{-7}\cdot\frac{newton\cdot sec}{m^2}$$

APPENDIX B

MBGF Calculations and Dimensionless Numbers

Joshua S. Nunez

3/15/02

$P_{Standard} := 14.696 psi$ Pressure of air at standard conditions

$T_{Standard} := 298 K$ Temperature of air at standard conditions

Critical Dimensions for MBGF

$D_{Exhaust} := 6 in$ Diameter of Exhaust pipe

$$A_{Exhaust} := \pi \cdot \frac{\left(D_{Exhaust}^{2}\right)}{4}$$

$A_{Exhaust} = 0.02 m^2$ Cross sectional area of exhaust

$D_{Inner} := 30 in$ Diameter of inner shell of MBGF

$$A_{Inner} := \pi \cdot \frac{\left(D_{Inner}^{2}\right)}{4}$$

$A_{Inner} = 0.46 m^2$ Cross sectional area of down-comer

$D_{Outer} := 36 in$ Diameter of outer shell of MBGF

$$A_{Outer} := \pi \cdot \frac{\left(D_{Outer}^{2}\right)}{4}$$

$A_{Outer} = 0.66 m^2$ Cross sectional area of entire MBGF

$A_{Total} := A_{Outer} - A_{Inner}$

$A_{Total} = 0.20 m^2$ Total cross sectional area of Inlet Gas

Temperatures of MBGF

$C\_K := 273$ Conversion from Celsius to Kelvin

$T_{Standard} := 298 K$ Temperature of air at standard conditions

$T_{Inlet} := (604 + C\_K) \cdot K$

$T_{Inlet} = 877.00K$ Inlet Gas temperature of MBGF

$T_{Exit} := (514 + C\_K) \cdot K$

$T_{Exit} = 787.00K$ Exit gas temperature of MBGF

Volumetric Flow Rates and Velocities

$Q_{Standard} := 200 \cdot \frac{ft^3}{min}$ Standard Volumetric Flow Rate leaving MBGF

$Q_{Standard} = 5.66 \frac{m^3}{min}$

$$V_{Inlet} := \frac{Q_{Standard} \cdot \left(\frac{T_{Inlet}}{T_{Standard}} \right)}{A_{Total}}$$

$V_{Inlet} = 1.38 \frac{m}{s}$ Face Velocity of gas at interfacial region

$$V_{Exit} := \frac{Q_{Standard} \cdot \left(\frac{T_{Exit}}{T_{Standard}} \right)}{A_{Inner}}$$

$V_{Exit} = 0.55 \frac{m}{s}$ Velocity of gas in Down-comer

MBGF Inlet Gas Charateristics

$T_{Inlet} = 877.00K$ Temperature of producer gas entering MBGF

$P_{Inlet} := P_{Standard} + \frac{1.5}{27.71} \cdot psi$

$P_{Inlet} = 14.75psi$ *Approx. pressure of the PG

$\rho_{InletPG} := \rho(T_{Inlet}, P_{Inlet})$

$\rho_{InletPG} = 0.40 \frac{kg}{m^3}$ Density of Producer gas entering MBGF

$\mu_{InletPG} := \mu(T_{Inlet})$

$\mu_{InletPG} = 3.93 \times 10^{-5} \frac{newton \cdot sec}{m^2}$ Kinamatic Viscosity of Producer Gas

MBGF Interior Gas Charateristics

$T_{Exit} = 787.00K$ Temperature of producer gas within the MBGF

$P_{Inlet} := P_{Standard} + \frac{1.5}{27.71} \cdot psi$

$P_{Inlet} = 14.75psi$ *Approx. pressure of the PG

$\rho_{ExitPG} := \rho(T_{Exit}, P_{Inlet})$

$\rho_{ExitPG} = 0.45 \frac{kg}{m^3}$ Density of Producer gas within the MBGF

$\mu_{ExitPG} := \mu(T_{Exit})$

$\mu_{ExitPG} = 3.64 \times 10^{-5} \frac{newton \cdot sec}{m^2}$ Kinamatic Viscosity of Gas within the MBGF

Determination of Stokes Number

$\rho_p := 600 \frac{kg}{m^3}$ Approx. particle density of fly ash

$D_p := 20 \cdot 10^{-6} \cdot m$ Approx. Diameter of particles

$Cu := 1$ Cunningham slip correction

$D_m := 3.84 mm$ Approx. Diameter of Filter Media

$Stokes\_Number := \frac{(\rho_p \cdot D_p^2 \cdot V_{Inlet} \cdot Cu)}{9 \cdot \mu_{InletPG} \cdot D_m}$

$Stokes\_Number = 0.24$ Stokes Number

Determination of Reynolds Number

$Re_{Inlet} := \frac{(\rho_{InletPG} \cdot V_{Inlet} \cdot D_m)}{\mu_{InletPG}}$

$Re_{Inlet} = 54.72$ Reynolds number at the interfacial region

$$Re_{Exit} := \frac{(\rho_{ExitPG} \cdot V_{Exit} \cdot D_m)}{\mu_{ExitPG}}$$

$Re_{Exit} = 25.93$ Reynolds number within the MBGF

Determination of Froude Number

$g = 9.81 \frac{m}{s^2}$ Gravitaitonal constant

$$Fr := \frac{(V_{Inlet}^2)}{g \cdot D_m}$$

$Fr = 50.89$ Froude number

Determination of Reynolds Number within *Inlet* Exhaust Duct

$$V_{Exhaust} := 2700 \frac{ft}{min}$$

$$Re_{Inlet} := \frac{(\rho_{InletPG} \cdot V_{Exhaust} \cdot D_{Exhaust})}{\mu_{InletPG}}$$

$Re_{Inlet} = 21515.70$ Reynolds number within the exhaust duct

Constants

Gas Constant for Air:

$F\_R \equiv 459.67$ Conversion from F to R

$R\_F \equiv -459.67$

$C\_K \equiv 273$ Conversion from C to K

$K\_C := -273$

$inH2O\_psi \equiv 27.71^{-1}$ Conversion from in H2O to psi

$psi\_inH2O \equiv 27.71$

$$R_{air} \equiv \frac{8.314 \frac{joule}{mole \cdot K}}{28.97 \cdot \frac{gm}{mole}}$$

$P_{stan} \equiv 1 \cdot atm$ Atm pressure:

$T_{stan} \equiv (77 + F\_R) \cdot R$ STP temperature

Empirical constants for air Cp calcs (Shapiro):

$\alpha \equiv 3.653$

$\beta \equiv -0.7428$

$\gamma \equiv 1.017$

$\delta \equiv -0.328$

$\varepsilon \equiv 0.02632$

$$Cp(T) \equiv R_{air} \cdot \left[\alpha + (\beta \cdot 10^{-3}) \cdot \left(\frac{T}{R}\right) + (\gamma \cdot 10^{-6}) \cdot \left(\frac{T}{R}\right)^2 + (\delta \cdot 10^{-9}) \cdot \left(\frac{T}{R}\right)^3 + (\varepsilon \cdot 10^{-12}) \cdot \left(\frac{T}{R}\right)^4 \right]$$

Ideal gas relations:

$$\rho(T,P) \equiv \frac{P}{R_{air} \cdot T}$$

Viscosity relations (air):

$$\mu(T) \equiv \left[52.584 + 0.262 \left(\frac{T}{R}\right) - 2.954\,10^{-5} \cdot \left(\frac{T}{R}\right)^2 \right] \cdot 10^{-7} \cdot \frac{newton \cdot sec}{m^2}$$

APPENDIX C

Test [I1-01]

Full line : Pre MBGF 25x overview (9/7/01 09:03)
Dashed line : Post MBGF 150x overview (9/7/01 09:20)

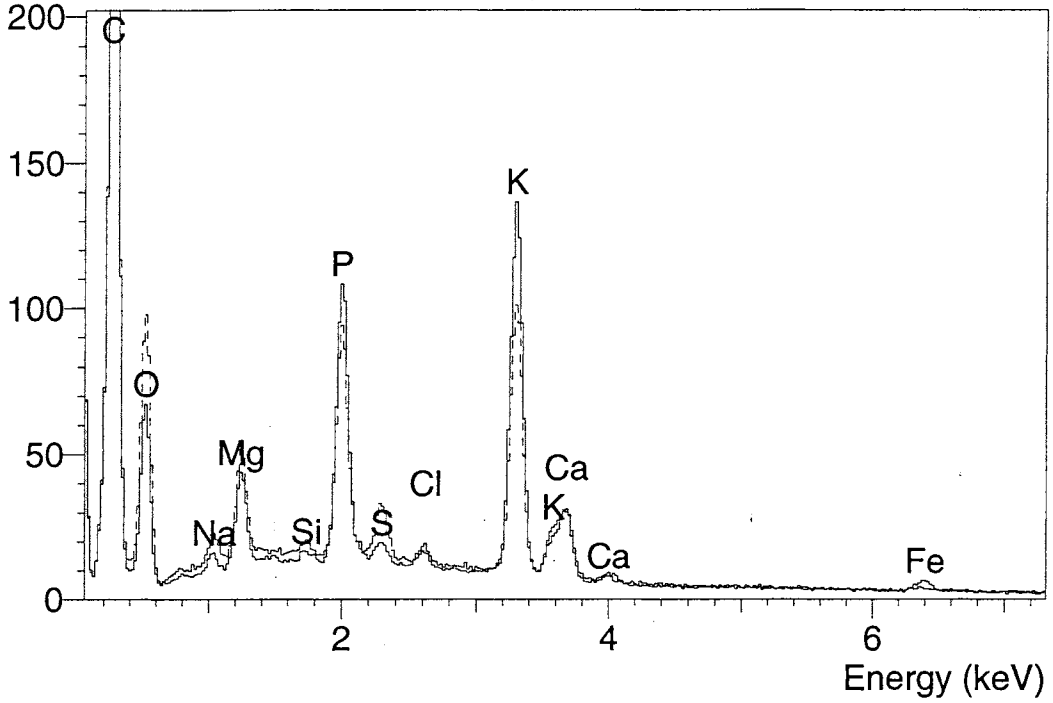

ID: Pre MBGF 25x overview

Elmt	Spect.	Element	Atomic
C K	ED	63.27	73.24
O K	ED	25.54	22.19
Na K	ED	0.26	0.16
Mg K	ED	1.20	0.68
Al K	ED	0.08	0.04
Si K	ED	0.08	0.04
P K	ED	2.76	1.24
S K	ED	0.24	0.10
Cl K	ED	0.19	0.07
K K	ED	5.09	1.81
Ca K	ED	0.93	0.32
Fe K	ED	0.39	0.10
Total		100.00	100.00

ID: Post MBGF 150x overview

Elmt	Spect.	Element	Atomic
C K	ED	60.28	69.54
O K	ED	30.81	26.69
Na K	ED	0.46	0.27
Mg K	ED	1.22	0.70
Al K	ED	0.03*	0.01*
Si K	ED	0.09	0.04
P K	ED	2.07	0.93
S K	ED	0.51	0.22
Cl K	ED	0.19	0.07
K K	ED	3.43	1.22
Ca K	ED	0.83	0.29
Fe K	ED	0.08	0.02
Total		100.00	100.00

Test [I1-02]

Full line : Pre MBGF 25x (9/12/01 09:51)
Dashed line : Post MBGF 25x (9/12/01 09:47) (Scaled)

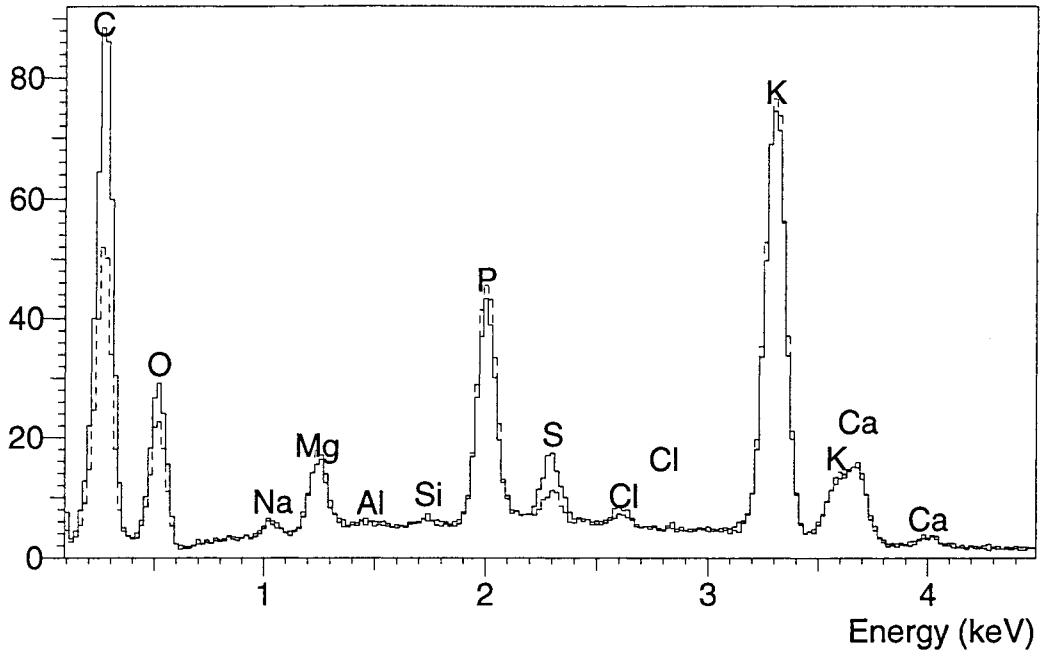

Spectrum label: Pre MBGF 25x

Elmt	Spect.	Element	Atomic
C K	ED	56.03	67.52
O K	ED	29.00	26.23
Na K	ED	0.29	0.18
Mg K	ED	1.20	0.71
Al K	ED	0.10	0.05
Si K	ED	0.07	0.04
P K	ED	2.89	1.35
S K	ED	0.87	0.39
Cl K	ED	0.17	0.07
K K	ED	7.96	2.95
Ca K	ED	1.30	0.47
Fe K	ED	0.12	0.03
Total		100.00	100.00

Spectrum label: Post MBGF 25x

Elmt	Spect.	Element	Atomic
C K	ED	49.70	62.86
O K	ED	29.51	28.02
Na K	ED	0.40	0.26
Mg K	ED	1.86	1.16
Al K	ED	0.07	0.04
Si K	ED	0.09	0.05
P K	ED	4.35	2.13
S K	ED	0.57	0.27
Cl K	ED	0.35	0.15
K K	ED	11.04	4.29
Ca K	ED	1.91	0.73
Fe K	ED	0.14	0.04
Total		100.00	100.00

Test [I2-01]

Full line : Inlet I2-01 300x (5/1/02 11:16)
Dashed line : Outlet I2-01 300x (5/1/02 11:24)

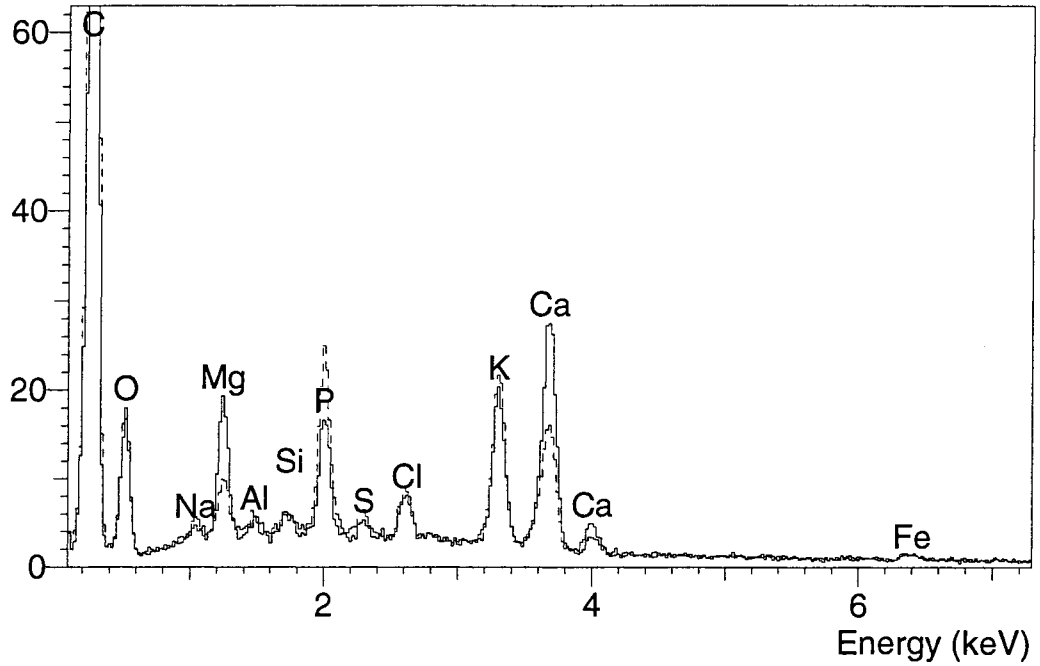

Pre MBGF 25x

Elmt	Spect.	Element	Atomic
C K	ED	56.03	67.52
O K	ED	29.00	26.23
Na K	ED	0.29	0.18
Mg K	ED	1.20	0.71
Al K	ED	0.10	0.05
Si K	ED	0.07	0.04
P K	ED	2.89	1.35
S K	ED	0.87	0.39
Cl K	ED	0.17	0.07
K K	ED	7.96	2.95
Ca K	ED	1.30	0.47
Fe K	ED	0.12	0.03
Total		100.00	100.00

Post MBGF 25x

Elmt	Spect.	Element	Atomic
C K	ED	49.70	62.86
O K	ED	29.51	28.02
Na K	ED	0.40	0.26
Mg K	ED	1.86	1.16
Al K	ED	0.07	0.04
Si K	ED	0.09	0.05
P K	ED	4.35	2.13
S K	ED	0.57	0.27
Cl K	ED	0.35	0.15
K K	ED	11.04	4.29
Ca K	ED	1.91	0.73
Fe K	ED	0.14	0.04
Total		100.00	100.00

Test[I2-02]

Full line : Inlet I2-02 50x (5/1/02 11:44)
Dashed line : Outlet I2-02 300x (5/1/02 11:37) (Scaled)

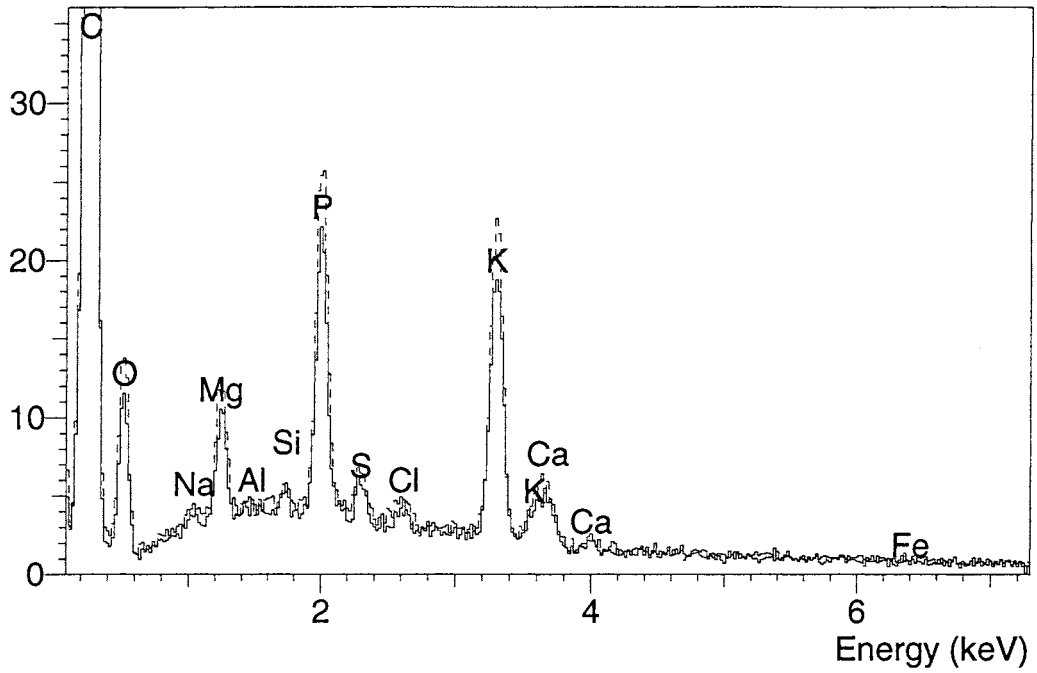

Pre MBGF 25x

Elmt	Spect.	Element	Atomic
Na K	ED	1.58	2.40
Mg K	ED	7.02	10.12
Al K	ED	0.64	0.83
Si K	ED	0.47	0.58
P K	ED	18.30	20.69
S K	ED	6.31	6.89
Cl K	ED	1.27	1.25
K K	ED	53.07	47.53
Ca K	ED	10.54	9.21
Fe K	ED	0.80	0.50
Total		100.00	100.00

Post MBGF 25x

Elmt	Spect.	Element	Atomic
Na K	ED	1.57	2.39
Mg K	ED	7.86	11.31
Al K	ED	0.35	0.45
Si K	ED	0.40	0.50
P K	ED	20.05	22.64
S K	ED	2.99	3.26
Cl K	ED	1.79	1.77
K K	ED	53.27	47.63
Ca K	ED	11.06	9.64
Fe K	ED	0.66	0.41
Total		100.00	100.00